Photon-Tagging Measurements at MAX-lab

Mohsen Meshkian

January 25, 2012

LTH, Lund University

Supervisor: Dr. Kevin Fissum

LUNDS UNIVERSITET
Lunds Tekniska Högskola

MAX-lab

Abstract

At the Tagged-Photon Facility at MAX-lab, the Swedish National Electron Accelerator Laboratory situated in Lund, bremsstrahlung photons are used for photonuclear experiments. The production takes place via an interaction between an energetic pulsed-stretched electron beam and a thin conducting foil. Determination of the energy and timing of the individual bremsstrahlung photons is made possible by a technique called "tagging". The so-called "tagging efficiency" is used to quantify the photon flux interacting with the target. It relates the number of photons striking the target to the number of electrons involved in their production. This parameter depends on several factors, such as collimator size and radiator tickness.

The aim of this thesis is to present the results of a comprehensive series measurements of the tagging efficiency for each channel in the tagger focal-plane detector performed using two different types of trigger during the June 2011 and September 2011 runperiods. Comparisons are made between the tagging efficiencies obtained using both triggers, demonstrating that the results are independent of the trigger type. Investigations for variations in the tagging efficiency as a function of when the event occurs (the so-called time-in-pulse) have also been performed. These investigations show that the results are independent of the relative timing of the event.

Contents

List of Abbreviations

ADC	Analog-to-Digital Converter
DAQ	Data AcQuisition
EGS	Electron-Gamma Shower
FO	Fan-Out
FP	Focal Plane
LINAC	LINear ACcelerator
Pb-glass	Lead glass
PMT	Photo-Multiplier Tube
PSR	Pulse-Stretcher Ring
QDC	Charge-to-Digital Converter
TDC	Time-to-Digital Converter
TiP	Time-in-Pulse

List of Figures

List of Tables

Populärvetenskaplig sammanfattning

MAX-lab är ett svenskt nationellt laboratorium beläget i Lund. I denna anläggning pågår det forskning inom ett stort antal områden. I anläggningen används det två linjära acceleratorer för att accelerera elektroner till nästan ljusets fart. Dessa elektroner injekteras därefter till tre ringar för att cirkulera i. Produktion av högenergetiska fotoner från de "lagrade" elektronerna är ett av användningsområdena på MAX-lab.

De högenergetiska fotonerna har de rätta egenskaparena för att påverka atomkärnor och göra studeringen av dessa möjligt. Kärnan kommer att påverkas när den träffas av en foton, och med hjälp av undersökning av resultatet kan man dra slutsatser om beståndsdelar i atomkärnan och vilka krfter och partiklar håller ihop atomkärnan. Kärnfotogruppen på MAX-lab är ansvarig för dessa experiment på MAX-lab.

Experiment och forskning med högenergetiska fotoner är oftast inte gjort med bara fotoner, utan också ett stort antal experimentella verktyg som är byggda kring produktionen. För att experimenten ska vara möjliga så måste fotonstrålen väldefinieras med hjälp av en kollimator. Kollimatorn är en cylinder av metall med ett hål i mitten som sedan placeras framför strålen. Fotoner som passerar hålet kommer till experimentområdet och resten absorberas av kollimatorn.

En viktig parameter i fotonukleära experiment är den så kallade "taggingeffektivitet" som är helt enkelt andelen av fotonerna som nås experimentområdet och interagerar med atomkärnorna. Med denna parametern kan man bestämma sannolikheten av de reaktioner som skall studeras. Denna parametern kan bestämmas med två olika elektroniska trigger. Dessa är kopplade till två olika detektorer, fokalplan detektorn och blyglas detektorn. Fokalplan detektorn registrerar elektroner medan blyglas detektorn registrerar fotoner. Taggingeffektivitet måste bli samma hela tiden oavsett vilken trigger som används.

I denna uppsats förklaras hur mätningar av taggingeffektivitet har genomförts och analysen av dessa mätningar har gjorts för båda trigger. Taggingeffektivitet har även analyserats för variation av pulshöjden med avseende på tiden i detektorerna. Pulsen delades in i mindre tidsintervaller och taggingeffektivitet mättes. Analysen av mätningar bevisar att taggingeffektivitet inte beror på typen av triggern och att det inte heller varierar med pulstiden.

Acknowledgements

It would not have been possible to perform and write this bachelor thesis without the help, continuous support, and patience of my kind supervisor. Therefore, first and foremost I'd like to thank Dr. Kevin Fissum for his assistance and invaluable advice throughout the project. I would also like to show my gratitude to Dr. Jason Brudvik for not hesitating in helping me with the analysis and providing me with new analysis techniques continuously. I would also thank Kurt Hansen, Lennart Isaksson, and the rest of the members of the photonuclear group for their welcoming and hospitality, and for making this new experience pleasant. I'm also grateful to Dr. William Briscoe, Dr. Grant O'Reilly, and the IRES students for being helpful with the data acquisition for my project. I dedicate this thesis to my wife who has made available her support in a number of ways.

1 Introduction

MAX-lab is the Swedish National Electron Accelerator Facility situated in Lund, Sweden. Its main components are an accelerator system and three storage rings. At MAX-lab, atoms and nuclei are investigated with the help of photons of a broad energy range.

The MAX I storage ring may be used as a pulse-stretcher ring (PSR) and thus can be employed to generate a continuous electron beam. By directing this beam towards a thin metallic foil, bremsstrahlung photons can be produced. In photonuclear experiments, these photons are used to probe the structure of nuclei.

In order to be sure that the trajectory of every bremsstrahlung photon intersects the target being probed, a collimator is placed downstream of the foil. Some fraction of the cone-shaped bremsstrahlung distribution passes through this collimator. This fraction of photons is commonly refered to as the "tagging efficiency".

The tagging efficiency is a very important component of every photonuclear experiment performed at MAX-lab as it plays a critical role in determining the absolute probability for a nuclear reaction to occur. The tagging efficiency must be measured carefully as changes in the steering of the electron beam or drifts in the power supplies connected to the magnets which control this steering may occur. This can result in changes in the number of photons which pass through the collimator. Thus, the tagging efficiency is measured both discretely (and absolutely) as well as continuously (and relatively). This thesis deals with the absolute measurements of the tagging efficiency performed during the June 2011 and September 2011 runperiods at MAX-lab.

2 Overview of MAX-lab

A schematic picture of the laboratory is shown in Fig. 1.

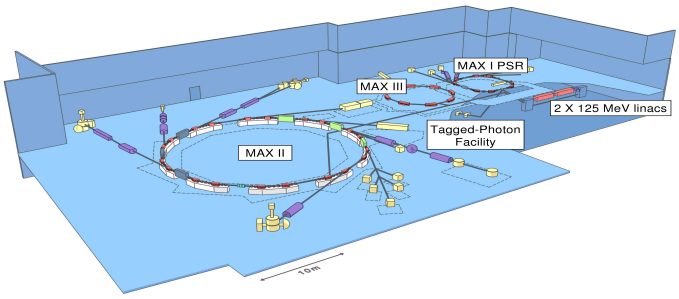

Figure 1: An overview of the MAX-lab research facility, featuring the LINACs and the three storage rings. Figure courtesy MAX-lab, modified by J. Brudvik.

A schematic picture of the MAX injector is shown in Fig. 2. A Rutherford gun is used as the electron source. The principle behind the operation of this gun is thermionic emission. The electron pulses have a length of 200 ns and a frequency of 10 Hz (after bunching). These 2 MeV electrons are then directed into two consecutive 5.2 m long LINACs, each of which provides a nominal

energy gain of 100 MeV. Unfortunately, this pulsed electron beam is not optimal for photonuclear experiments. Instead, it is preferable to have a continuous electron beam with a lower continuous current.

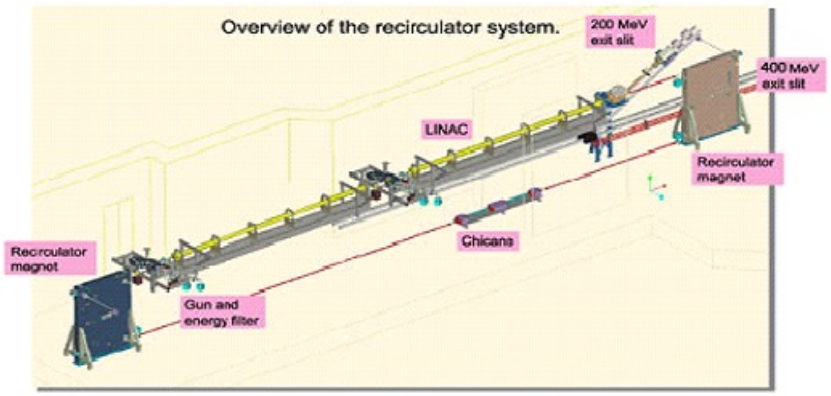

Figure 2: An overview of the electron gun and the two LINACs. Figure courtesy MAX-lab.

The electron beam is then injected into the MAX I ring. MAX I has a circumference of 32.4 m which corresponds to an orbit time of 108 ns for the electrons which travel with approximately speed of light. As previously mentioned, MAX I can be operated as a PSR. In this mode, the 200 ns electron bunches enter MAX I, are "captured" in the ring, and then slowly extracted. This results in an almost continuous beam. The stretched beam from the MAX I ring is then transported via a beamline to the Tagged-Photon Facility (TPF). This transport beamline contains several bending magnets which may also be used to measure the electron-beam energy.

3 The Photon-Tagging System

3.1 The Electron Beam and Focal-plane Detector

The stretched electron beam is directed towards a thin metal foil known as a "radiator". Some of the incoming electrons undergo interactions with the nuclei in the foil. As a result, bremsstrahlung photons are radiated. A continuous distribution of bremsstrahlung photon energies is produced, ranging from zero up to the incident electron-beam energy. A typical bremsstrahlung spectrum is shown in Fig. 3, corresponding to a 300 μm Al radiator and a 192.5 MeV

electron beam.

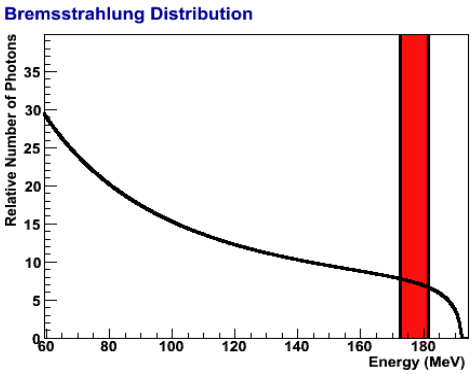

Figure 3: A bremsstrahlung distribution. A typical tagged-photon energy range is superimposed. Figure courtesy M. Litwack.

A schematic overview of a photon-tagger spectrometer is shown in Fig. 4.

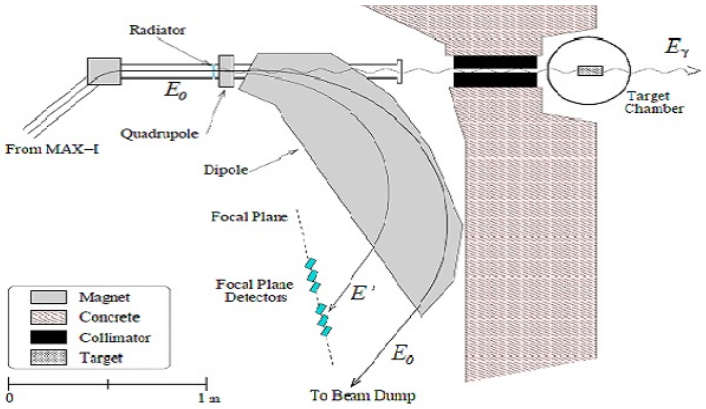

Figure 4: A photon-tagging spectrometer. The figure illustrates the principle of a photon-tagging measurement. Figure courtesy M. Karlsson.

In the bremsstrahlung process, the incident electron (with energy E_0) may radiate a bremsstrahlung photon (with energy E_γ). If the recoiling electron has energy E', the energy of the photon is given by

$$E_\gamma = E_0 - E'. \tag{1}$$

The energy of the incoming electron beam is known. To measure the energy of the recoiling electron, a dipole magnet may be located immediately downstream of the radiator. The magnetic field of the dipole does not affect the photons, but instead directs the recoiling electrons falling within its acceptance onto its focal plane (the vertical shaded bar in Fig. 3).

The trajectory of the recoiling electrons in the dipole field of the magnet is curved due to the Lorentz force. The tagger dipole is constructed so that there

is a linear dependence between the position of the focal-plane detectors and the residual electron energy E'. In a perfect dipole field, different electron energies result in circular paths with different radii given by

$$R = \frac{\beta E'}{ecB}, \tag{2}$$

where R is the radius of the trajectory, e is the charge of the electron, B is the strength of the magnetic field, and $\beta = \frac{v}{c}$. Energetic electrons follow a trajectory with a larger radius than those that have lost much of their energy. Electrons that do not produce a photon in the radiator are so energetic that they simply pass by the focal plane and are directed onto a Faraday cup which provides a measure of the electron-beam current.

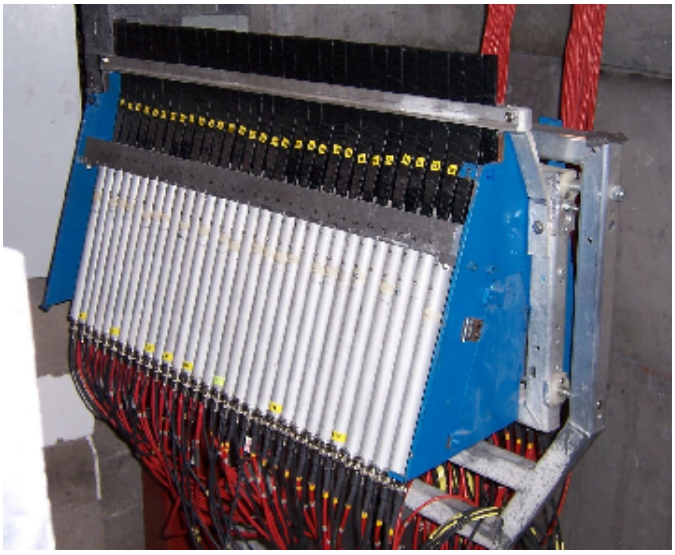

Figure 5: The focal plane array used at MAX-lab. Figure courtesy K. Fissum.

The focal plane at MAX-lab consists of 63 plastic-scintillator detectors placed on a movable array next to the exit window of the dipole magnet (see Fig. 5). The focal plane is 100% efficient for the purpose of detecting recoiling electrons. Since the beam energy is known and the magnetic field of the tagger magnet is known, the energy of the post-bremsstrahlung recoiling electron may be determined simply by locating the detector in the focal-plane array that was hit. The photon energy may then be reconstructed using Eq. (1). The physical width of the electron detectors defines the energy resolution of the focal-plane hodoscope.

Since background radiation (mainly gamma radiation from beam-activated shielding) can strike a focal-plane detector and result in a signal, the focal plane is arranged into coincident front-plane and back-plane "channels" so that only signals existing simultaneously in the front-plane and back-plane scintillators result in a trigger. In this manner, only charged particles such as energetic recoiling electrons are selected and background photons (which cannot create coincidences between the front and back planes) are greatly suppressed. The 63 plastic-scintillator detectors composing the focal-plane array are thus arranged into two parallel rows, each having 31 detectors.

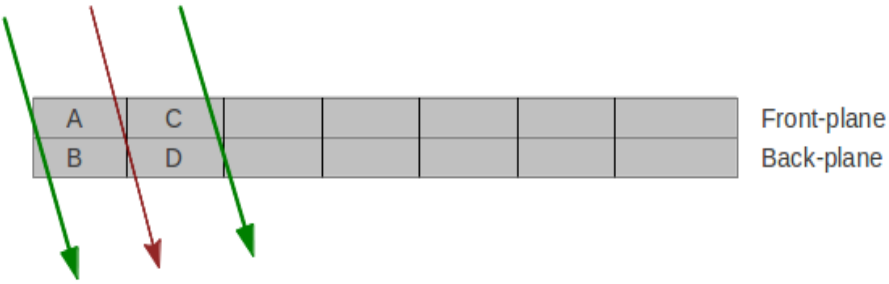

Figure 6: Focal-plane channel definition.

The focal-plane channels are simply defined as the physical overlap between the front- and back-plane scintillators. During the experiments the scintillators were operated in the 100% overlap mode (see Fig. 6). Thus, it was more likely that electrons passed through the even channels since they physically subtend more solid angle.

Fig. 6 illustrates the front- and back-plane scintillators in the focal plane. Four FP detectors are labeled A, B, C, and D. If an electron passes through either of the two regions between the green arrows and the red one, a coincidence is formed between the front- and the back-plane scintillators. Channel zero is defined as the coincidence between A and B, while the coincidence between C and D results in channel two. If the electron passes through the scintillator planes as the red arrow, i.e. through A and D, then A and D are in coincidence with each other. This corresponds to a hit in channel 1.

This purely geometric effect results in the picket-fence structure shown in Fig. 7, which is known as the "odd-even" effect. Due to this effect, only the even channels were considered with analysis.

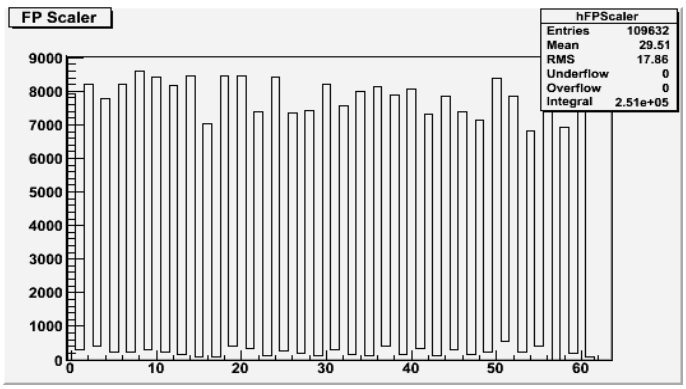

Figure 7: An FP OR scaler histogram from a trigger run.

3.2 The Photon Beam and Pb-glass Detector

As previously mentioned, bremsstrahlung photons are emitted in a conical distribution in the direction of the incident electron beam.

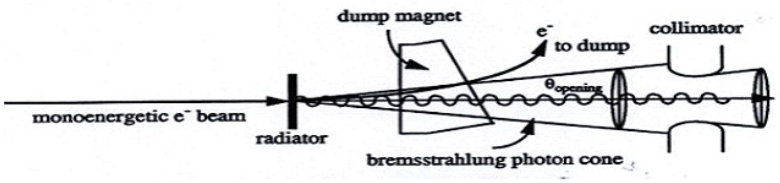

Figure 8: Overview of the bremsstrahlung cone leaving the radiator and entering the collimator. Figure courtesy K. Fissum.

The energy of the incident electrons defines the opening angle of the cone according to

$$\theta_{\text{opening}} \approx \frac{1}{\gamma} = \frac{1}{\frac{E_0}{m_e c^2}}, \tag{3}$$

where E_0 is the energy of the electron, m_e is the electron mass, and γ is the gamma factor for the incoming electrons.

Since the target is often located well downstream of the radiator, the spread of the cone may be large enough so that some fraction of the bremsstrahlung photons can actually miss the target. This would make the experiment impossible to normalize[1], since the incident photon flux must be known. Because of this, a collimator is situated after the spectrometer magnet (see Fig. 8). This defines the beam size and ensures that the path of every single bremsstrahlung photon will intersect the target.

For tagging measurements at MAX-lab, a Pb-glass detector is used for detecting photons at very low rates. Pb-glass is 100% efficient at detecting photons at tens of Hz. The Pb-glass scintillator works as follows: a high-energy photon is converted to an energetic electron-positron pair which then emits further energetic bremsstrahlung photons. These, in turn, will convert into electron-positron pairs, and the process continues. This cascade of Pair Production, Compton Scattering, and the Photoelectric Effect is known as an electron-gamma "shower" (EGS). Within the Pb-glass scintillator, the EGS results in the emission of a flash of light which is proportional to the energy of the original incident photon. The flash of light is transformed into an electrical signal by the photomultiplier (PMT) connected to the Pb-glass scintillator, and this signal is then used for data aquisition and analysis.

[1] The cross section is proportional to the yield divided by the number of incident photons.

4 Tagging Efficiency

4.1 Overview

Since the beam is collimated[2], not every electron registered in the focal-plane detectors will have a corresponding photon at the target position. The tagging efficiency ϵ_{tagg} is defined as the ratio of photons striking the target to the number of electrons incident on the focal plane, and is given by

$$\epsilon_{\text{tagg}} = \frac{N_\gamma}{N_{fp}}, \tag{4}$$

where N_γ is the number of bremsstrahlung photons passing through the collimator and N_{fp} represents the number of recoiling-electron events that are detected by the focal plane. Since only the number of electrons registered by the focal plane may be counted during an experiment, another means must be used to determine the number of photons incident upon the target.

Clearly, the size of the collimator affects the tagging efficiency strongly. The smaller the collimator, the lower the tagging efficiency. Further, the tagging efficiency is higher for photons with higher energies, because the opening angle of the bremsstrahlung cone is smaller (recall Eq. (3)), and thus more photons pass through the hole.

Processes within the radiator can also lower the tagging efficiency. For example, the electron beam has a finite size. Also, when electrons pass through the foil, they will undergo Coulomb multiple scattering. This will further increase the size of the electron beam and in turn increase the angular spread of the photons. A larger photon beam results in more photons being collimated, and the tagging efficiency is thus lowered. Another effect in the radiator which lowers the tagging efficiency is Møller scattering. When Møller scattering occurs, additional atomic electrons are liberated from the radiator atoms by the highly energetic incident electrons. This decreases the tagging efficiency since the process results in additional electrons that are counted by the focal-plane detectors without any photons being produced.

4.2 Measurements

Tagging-efficiency measurements are usually performed once per a day for both FP OR and Pb-glass triggers (see below), each of which must be background corrected. To start the measurement, the Pb-glass must be placed into the beam to detect the bremsstrahlung photons. The beam must be greatly reduced in intensity as compared to production rates to avoid pileup in the Pb-glass detector. To measure the tagging efficiency, the electron-beam rate is about 50 Hz across the focal plane. Regardless of the type of trigger used, a beam-on measurement must be at least 45 minutes for 3% statistical precision in the data. After the measurement, a 15 minute beam-off measurement is performed for the background correction. The major source of background is photons from activated shielding in the experimental hall.

To be able to record the signals from the focal-plane array and the Pb-glass detector during a tagging-efficiency run, electronics are used. Two different

[2]There are also other second-order effects, such as Coulomb multiple scattering in the radiator, Møller electrons, and background in the focal-plane detectors.

triggers convert the signals from the detectors to analyzable data. Note that while the electronics for signal conversion for each of these two triggers are different, the results are independent of the type of trigger used.

4.2.1 FP OR Trigger

The focal-plane signals are used to trigger the DAQ when using the FP OR trigger (see Fig. 9).

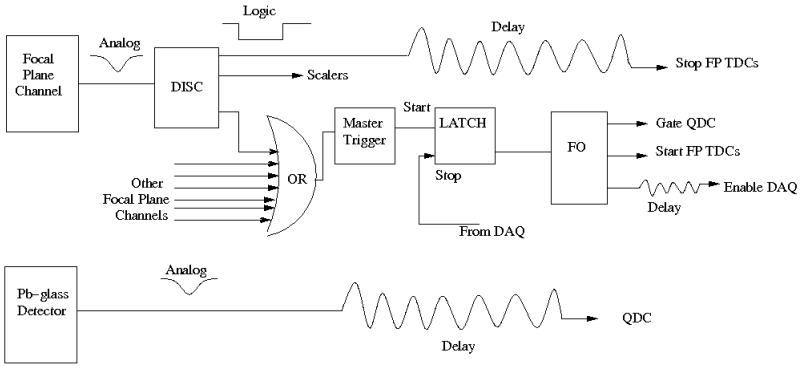

Figure 9: An illustration of the electronics for the FP OR trigger. Figure courtesy M. Litwack.

When a focal-plane channel is hit by an electron, an analog signal is sent to a discriminator. This produces three identical logic signals, each of which are used differently. One signal (after an appropriate delay[3]) is sent to stop the FP TDC, another is sent to the corresponding electron scaler, and the final copy is sent to an OR module. Note that signals from other FP channels may also be present at the OR module. This FP OR signal leaves the OR for the Master Trigger Unit which then passes it to the LATCH. The LATCH accepts only one signal at a time. Other signals will be prevented from passing until the present signal has been processed. The signal from the LATCH is passed to a fanout module which produces three identical copies of the incident signal. One copy is used to gate the Pb-glass QDC, another copy is used to start the FP TDCs, and the third (slightly delayed) copy enables the DAQ. After the DAQ has processed the entire event, it will send a stop signal to the LATCH so that further FP OR signals will be allowed to pass.

Simultaneous to the signal from the FP OR trigger, a bremsstrahlung photon may cause a reaction in the Pb-glass detector resulting in an analog signal from the PMT. This signal is sent to the Pb-glass QDC, and is delayed so that it arrives within the QDC gate signal. In order to determine the charge carried by the signal from the Pb-glass detector, the gate signal specifies the time range over which the analog signal should be integrated (see Fig. 10).

[3] This is due to the fact that the stop signal for the FP TDC must arrive at the TDC after the start signal.

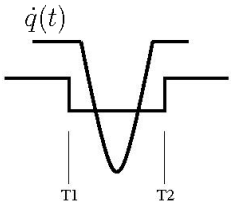

Figure 10: Relative timing of signal and gate at the QDC.

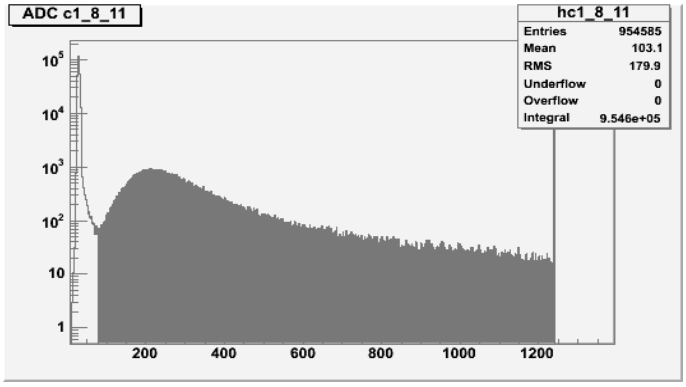

Figure 11: A typical QDC plot from the FP OR trigger. Note the logarithmic scale.

The charge carried by the signal is given by Eq. (5).

$$Q = \int_{T_1}^{T_2} \dot{q}(t)dt. \tag{5}$$

Data collected using the FP OR trigger will eventually result in a QDC plot, such as that shown in Fig. 11. The signals from the electrons which do not have a corresponding photon result in a sharp peak, known as a "pedestal". The pedestal in Fig. 11 occurs roughly at channel 25 and is unshaded. The shaded portion of the plot corresponds to the total number of photons detected in the Pb-glass. The small spike above channel 1200 is due to overflow[4]. The total number of electrons is simply the integral of the entire QDC plot since every electron triggered the DAQ. The tagging efficiency can then be determined as the ratio of the integral of the distribution corresponding to the photons (the gray part) to the total integral of the QDC spectrum.

4.2.2 Pb-glass Trigger

When using the Pb-glass trigger (see Fig. 12), the Pb-glass detector will trigger the DAQ. When a photon is detected in this detector, the PMT sends an analog signal to a fanout module, and two identical copies are created for different

[4]Highly energetic photons which do not fall within the energy range of the QDC will be placed in the overflow bin.

purposes. One signal is delayed and sent to the Pb-glass QDC, while the other is sent to a discriminator to be converted into a logic signal. This signal is delivered to the Master Trigger Unit which in turn passes it to the LATCH. The LATCH accepts only one signal at a time. Other signals will be prevented from passing until the present signal has been processed. The signal from the LATCH is passed to a fanout module which produces three identical copies of the incident signal. One copy is used to gate the Pb-glass QDC, another copy is used to start the FP TDCs, and the third (slightly delayed) copy enables the DAQ. After the DAQ has processed the entire event, it will send a stop signal to the LATCH so that further Pb-glass signals will be allowed to pass.

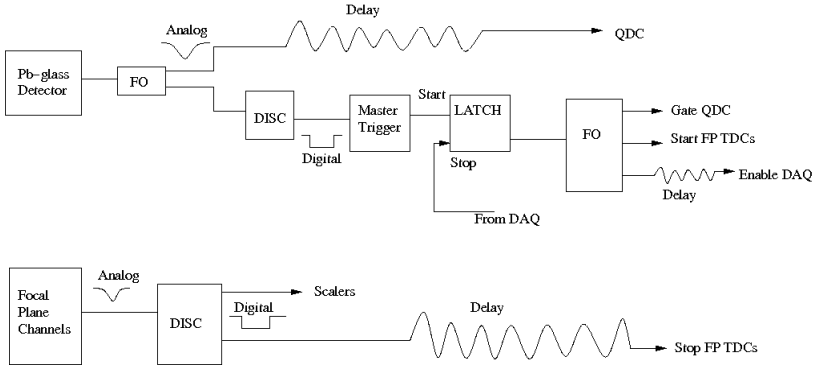

Figure 12: An illustration of the electronics for the Pb-glass trigger. Figure courtesy M. Litwack.

Furthermore, an analog signal is produced when an electron hits a focal-plane channel. This signal is split into two identical logic signals, one for the focal-plane scaler and the other to stop the FP TDC. The stop signal will also be delayed in this case, simply because the stop signal must come after the start signal.

Since every photon starts the focal-plane TDCs, the total number of photons corresponding to a given channel is just the total number of counts in the spike in the focal-plane TDC. The total number of electrons in a given focal-plane channel may be obtained from the focal-plane scalers. The tagging efficiency is again the ratio of these two quantities.

4.3 TiP Distribution

The Time-in-Pulse distribution (TiP) illustrates the relative timing of an event. It is formed in the following manner. A clock running at a frequency of 10 MHz is directed onto an uninhibited scaler. This scaler is cleared every 100 ms in conjunction with the 10 Hz machine trigger. Meanwhile, in conjunction with every event, it is read. By histogramming the results of this read, the beam profile is measured. The electronics used are shown in Fig. 13.

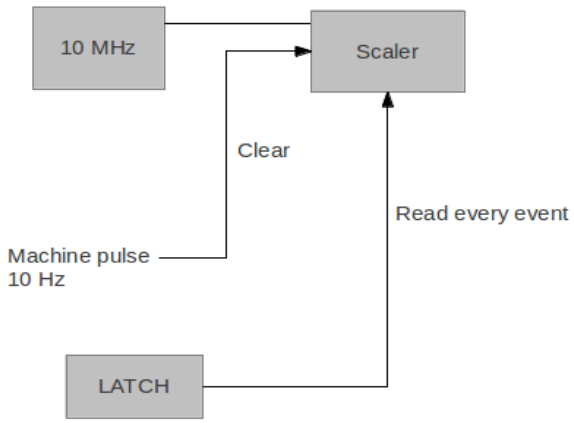

Figure 13: The electronics used for determining the TiP distribution.

A typical TiP distribution is shown in Fig. 14. The top panel shows the TiP distribution for the FP OR trigger and the bottom panel shows the same distribution for the Pb-glass trigger. During the tagging-efficiency experiment, two long runs were performed for each of the triggers. The tagging efficiency for the FP OR trigger run was then analyzed by dividing the TiP distribution into time intervals and examining the tagging efficiency for changes in these intervals.

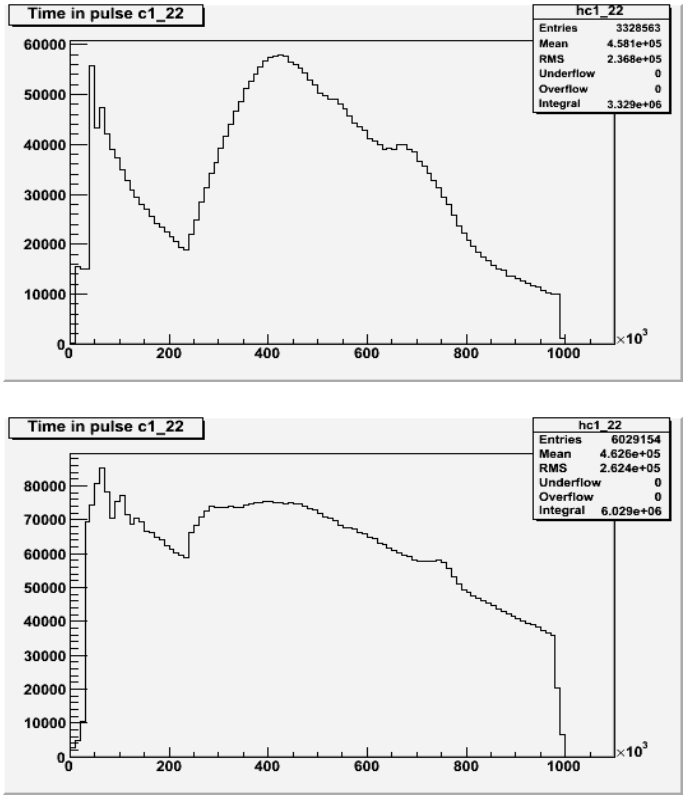

Figure 14: (top panel) TiP distribution for the FP OR trigger. (bottom panel) TiP distribution for the Pb-glass trigger.

As the time between beam pulses is 100 ms, the scales of the above spectra are 100 ns per channel.

4.4 Sample Spectra

4.4.1 FP TDC Histogram

4.4.1.1 FP OR Trigger

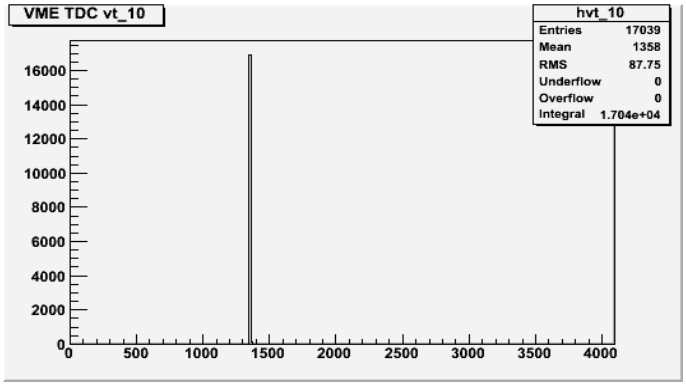

Figure 15: FP TDC spectrum for channel 10 for the an FP OR trigger.

The time difference between the FP start and the FP stop signal in the FP OR trigger is represented by the FP TDC histogram shown in Fig. 15. With such a trigger, the same electron starts and stops the TDC, and thus the position of the peak represents the time delay caused by the circuit cable. The number of events in the FP TDC histogram corresponds to the number of electrons in that particular channel.

4.4.1.2 Pb-glass Trigger

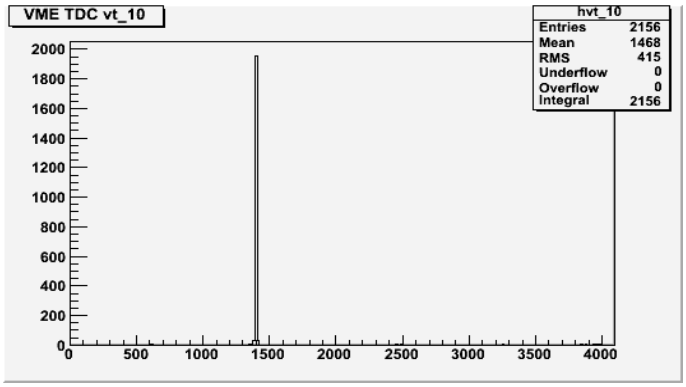

Figure 16: FP TDC spectrum for channel 10 for the Pb-glass trigger.

The time difference between the FP start and the FP stop signal in the Pb-glass trigger is represented by the FP TDC histogram shown in Fig. 16. With such a trigger, the photon starts the TDC and the electron stops it. Thus, the position of the peak represents the time delay caused by the circuit cable. The number of

counts in the FP TDC histogram corresponds to the number of electron-photon event pairs.

4.4.2 QDC Histograms

4.4.2.1 FP OR Trigger

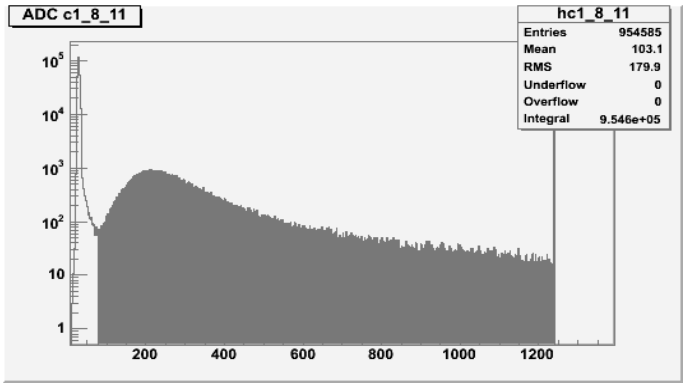

Figure 17: A typical QDC histogram for the FP OR trigger.

The charge of the signal delivered from the PMT connected to the Pb-glass is proportional to the energy deposited by the photon in the detector. A typical QDC histogram for the Pb-glass trigger is shown Fig. 17.

The QDC histogram may be divided into three parts: the pedestal (the spike at about channel 25), the overflow (the spike at about channel 1300) and the photon-energy distribution. The pedestal represents the electrons in the focal-plane that have no corresponding bremsstrahlung photons. Thus, the QDC integrates only the offset current (recall Fig. 10), resulting in the same value every time. When histogrammed, a spike at channel 25 results. When extremely energetic photons from the bremsstrahlung tip deposit more energy than the QDC is calibrated to handle, a count is placed in the overflow bin. When histogrammed, a spike at channel 1300 results. "Normal" photons deposit a full range of energies in the QDC (see the shaded gray region of Fig. 17).

4.4.2.2 Pb-glass Trigger

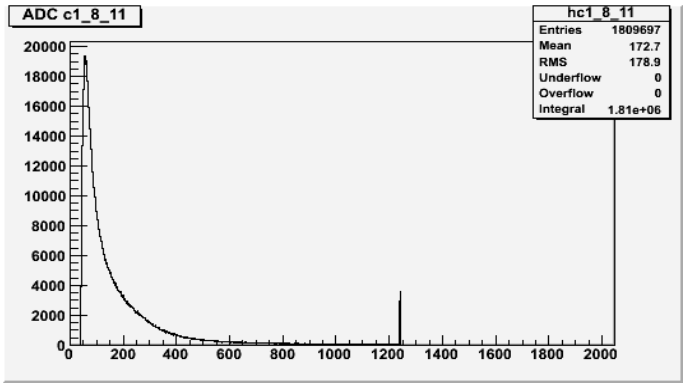

Figure 18: The QDC histogram for a Pb-glass trigger run.

When the Pb-glass trigger is used, the QDC will be gated whenever a photon strikes the Pb-glass detector. Thus, there will always an event to integrate, and no pedestal will appear. When extremely energetic photons from the bremsstrahlung tip deposit more energy than the QDC is calibrated to handle, a count is placed in the overflow bin. When histogrammed, a spike at about channel 1300 results. "Normal" photons deposit a full range of energies in the QDC. Thus, a typical bremsstrahlung distribution will be produced when the energy values of every photon incident upon the Pb-glass detector are histogrammed (see Fig. 18).

4.5 FP Scalers

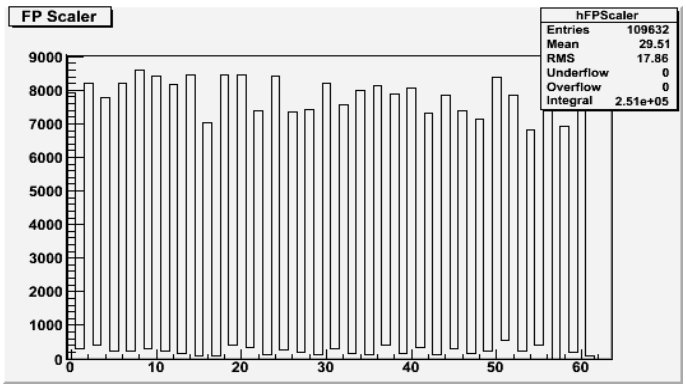

Figure 19: The FP scaler histogram from a Pb-glass trigger run.

Every time a FP channel is hit, a signal is sent to a corresponding scaler. These scalers count each hit. The number of electrons in every channel may therefore be presented using an FP scaler histogram, see Fig. 19. The number of electrons in a given channel is equal to the content of the corresponding bin in the his-

togram, while the total number of electrons in the focal plane is determined by the integral of the entire FP scaler histogram.

4.6 Experiment

Week	Activity
1	Background research
2	Background research
3	Production of tagging-effciency data
4	Production of tagging-effciency data
5	Production of tagging-effciency data
6	Production of tagging-effciency data
7	Production of tagging-effciency data
8	Production of tagging-effciency data
9	Production of tagging-effciency data
10	Production of tagging-effciency data
11	Analysis of tagging-effciency data
12	Analysis of tagging-effciency data
13	Writing of thesis
14	Writing of thesis
15	Preparing of presentation

Table 1: Week-by-week project summary.

5 Analysis

5.1 Tagging Efficiency Comparison

5.1.1 FP OR Trigger

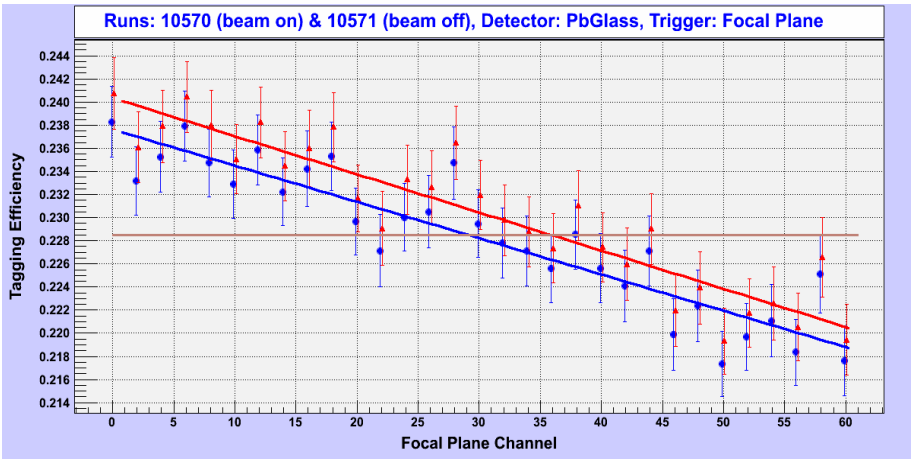

Figure 20: Tagging Efficiency for the FP OR trigger.

For each trigger type, two different tagging-efficiency measurements were performed, one for "beam on" and one for "beam off". Fig. 20 shows a typical tagging-efficiency plot, in this case for run numbers 10570 and 10571. The blue data points correspond to the tagging efficiency without background correction while the red data points correspond to the background-corrected values. The horizontal pink line corresponds to a crude average of the results. It is clear that a crude average is not sufficient to describe the results. Since the lowest-energy electrons are detected in the lowest channels, the corresponding photons have the highest energy. This results in an increase in the tagging efficiency for the reasons detailed in Chapt. 3, and thus the negative slope of the plot in Fig. 20.

5.1.2 Pb-glass Trigger

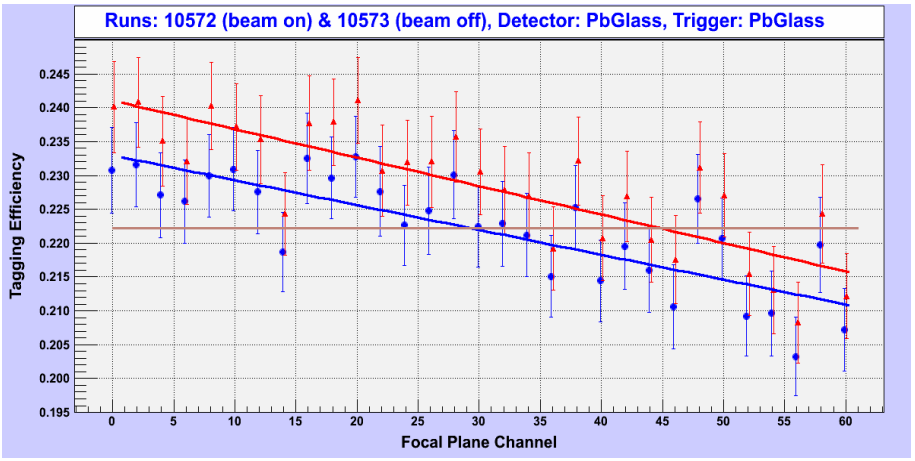

Figure 21: Tagging Efficiency for the Pb-glass trigger.

For each trigger type, two different tagging-efficiency measurements were performed, one for "beam on" and one for "beam off". Fig. 21 shows a typical tagging-efficiency plot, in this case for run numbers 10572 and 10573. The blue data points correspond to the tagging efficiency without background correction while the red data points correspond to the background-corrected values. The horizontal pink line corresponds to a crude average of the results. It is clear that a crude average is not sufficient to describe the results. Since the lowest-energy electrons are detected in the lowest channels, the corresponding photons have the highest energies. This results in an increase in the tagging efficiency for the reasons detailed in Chapt. 3, and thus the negative slope of the plot in Fig. 21.

5.1.3 Comparison of FP OR and Pb-glass Triggers

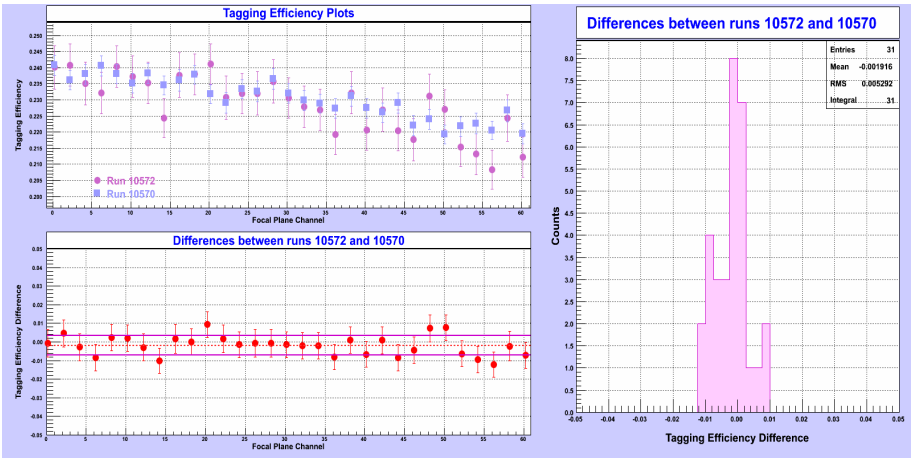

Figure 22: A comparison between the FP OR and Pb-glass triggers.

Comparisons between the tagging efficiencies measured for the FP OR trigger and the Pb-glass trigger were performed. In the ideal case, this difference (when histogrammed) would be a δ-function centered at zero. In reality, statistics and systematic uncertainties play a role. Thus, the δ-function is smeared to a Gaussian distribution which may also be slightly offset from zero. Fig. 22 shows the comparison between the FP OR run 10570 and the Pb-glass run 10572. See Appendix B for a complete set of results.

5.2 Tagging-Efficiency Extraction

5.2.1 FP OR Trigger

For the FP OR trigger, the number of photons is determined by integrating from the minimum to the overflow channel in the Pb-glass QDC. The number of electrons can be determined in several ways. The total integral of the QDC histogram corresponds to the number of electrons. This can also be found by integrating the spike in the TDC histogram. The final method is to examine the electron scalers in the FP scaler histogram.

5.2.2 Pb-glass Trigger

The calculation of the tagging efficiency for Pb-glass data is slightly different from that for the FP OR trigger data. In the TDC histogram, the peak represents the photon counts, and thus integrating the peak results in the number of photons. The number of electrons can only be determined by examining the electron scalers in the FP scaler histogram.

6 Results

6.1 FP OR Trigger

Fig. 23 (top panel) shows the background-corrected tagging efficiency for the FP OR trigger for tagger channel 12 as a function of run number. Statistical uncertainties are shown. Fig. 23 (bottom panel) shows the projection of these values onto the tagging-efficiency axis. As expected, there is no time evolution in the tagging efficiency within statistical uncertainty. See Appendix C for a complete set of results.

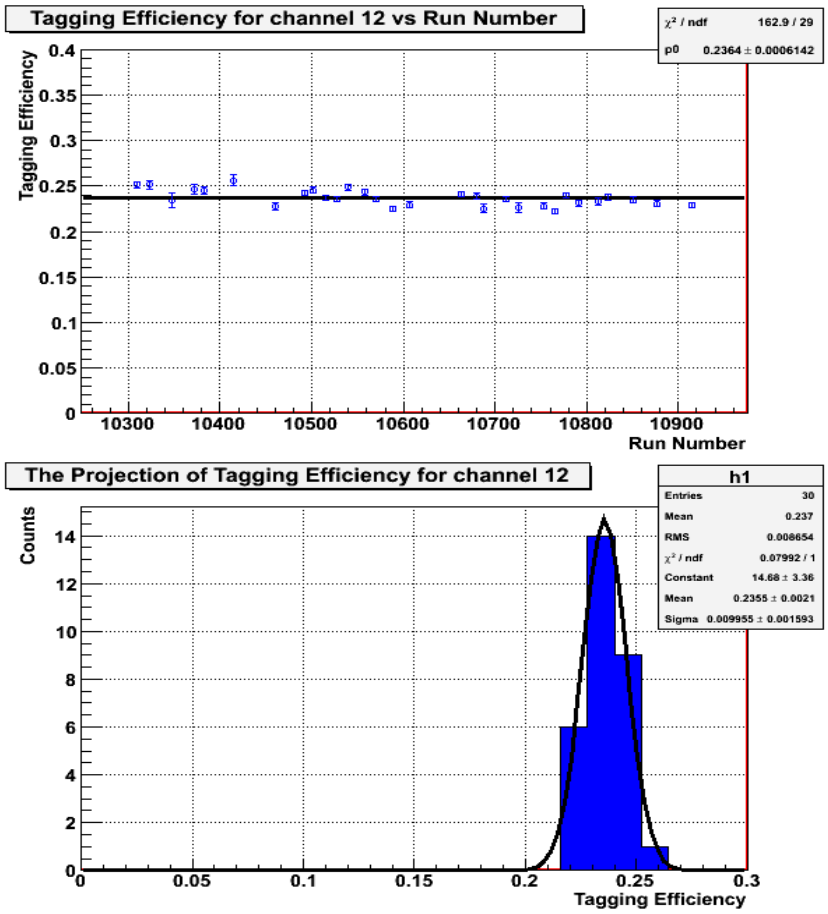

Figure 23: Selected FP OR results for channel 12. (top panel) Tagging Efficiency for the FP OR trigger for channel 12 vs. run number. (bottom panel) The projection of the tagging efficiency for channel 12. The tagging efficiency was 0.237 ± 0.009.

6.2 Pb-glass Trigger

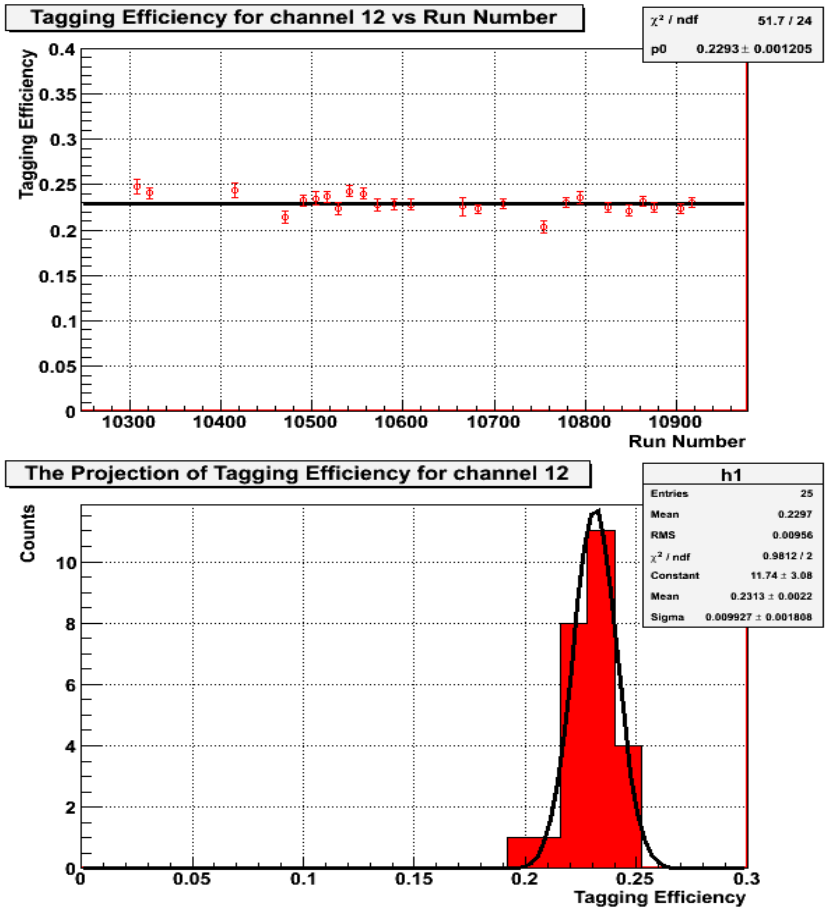

Figure 24: Selected Pb-glass results for channel 12. (top panel) Tagging efficiency for the Pb-glass trigger for channel 12 vs. run number. (bottom panel) The projection of tagging efficiency for Pb-glass trigger for channel 12. The tagging efficiency was 0.230 ± 0.010.

Fig. 24 (top panel) shows the background-corrected tagging efficiency for the Pb-glass trigger for tagger channel 12 as a function of run number. Statistical uncertainties are shown. Fig. 24 (bottom panel) shows the projection of these values onto the tagging-efficiency axis. As expected, there is no time evolution in the tagging efficiency within statistical uncertainty. See Appendix D for a complete set of results.

6.3 Data Set and Final Tagging Efficiency

Channel	ϵ_{tagg}(FP OR)	ϵ_{tagg}(Pb-glass)	Agreement
0	0.240±0.008	0.239±.009	Yes
2	0.239±0.009	0.233±0.007	Yes
4	0.240±0.008	0.233±0.009	Yes
6	0.240±0.008	0.232±0.009	Yes
8	0.240±0.008	0.230±0.008	Yes
10	0.236±0.008	0.230±0.010	Yes
12	0.237±0.009	0.230±0.010	Yes
14	0.236±0.007	0.227±0.009	Yes
16	0.236±0.008	0.230±0.009	Yes
18	0.235±0.009	0.230±0.010	Yes
20	0.235±0.008	0.230±0.010	Yes
22	0.236±0.007	0.231±0.008	Yes
24	0.235±0.008	0.230±0.010	Yes
26	0.236±0.009	0.230±0.010	Yes
28	0.235±0.007	0.230±0.006	Yes
30	0.233±0.006	0.227±0.010	Yes
32	0.234±0.007	0.230±0.009	Yes
34	0.232±0.007	0.227±0.010	Yes
36	0.230±0.008	0.224±0.009	Yes
38	0.230±0.006	0.224±0.009	Yes
40	0.230±0.008	0.224±0.010	Yes
42	0.230±0.008	0.220±0.010	Yes
44	0.230±0.008	0.222±0.009	Yes
46	0.224±0.008	0.217±0.008	Yes
48	0.227±0.007	0.223±0.008	Yes
50	0.224±0.007	0.217±0.010	Yes
52	0.222±0.007	0.215±0.009	Yes
54	0.225±0.006	0.220±0.008	Yes
56	0.220±0.006	0.213±0.008	Yes
58	0.230±0.008	0.224±0.009	Yes
60	0.220±0.007	0.213±0.007	Yes

Table 2: A summary of the measured tagging efficiencies for both triggers.

The tagging efficiencies measured for each channel together with their statistical uncertainties are shown in Table 2.

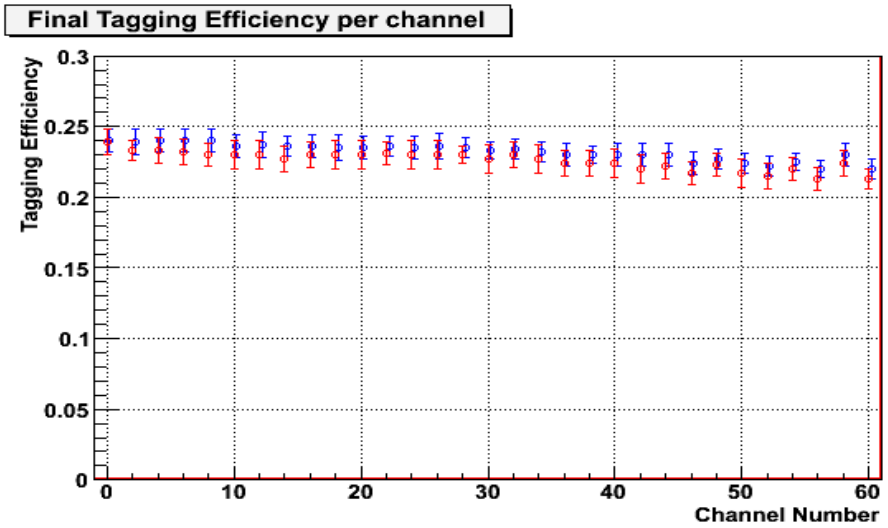

Figure 25: The tagging-efficiency results plotted for the FP OR (blue) and Pb-glass triggers (red).

The time evolution of the tagging efficiency for both triggers is plotted in Fig. 25. There is evidence of a small systematic shift between the results obtained with the different trigger types.

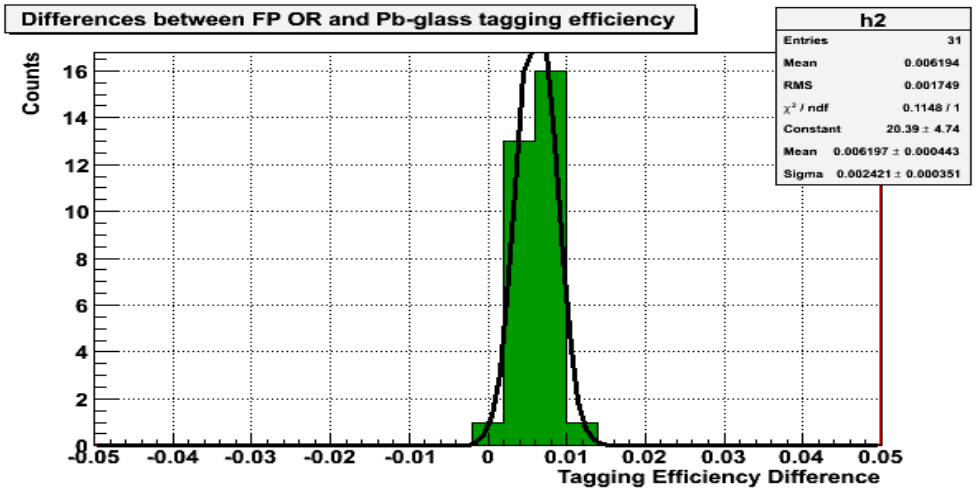

Figure 26: The difference between the FP OR and the Pb-glass tagging efficiency.

Figure 26 presents a histogram of the differences between the tagging efficiencies obtained for each of the two trigger types. Based upon this histogram, a systematic uncertainty in the measurements of $\pm 0.6\%$ is assigned.

6.4 TiP cutting and Tagging Efficiency

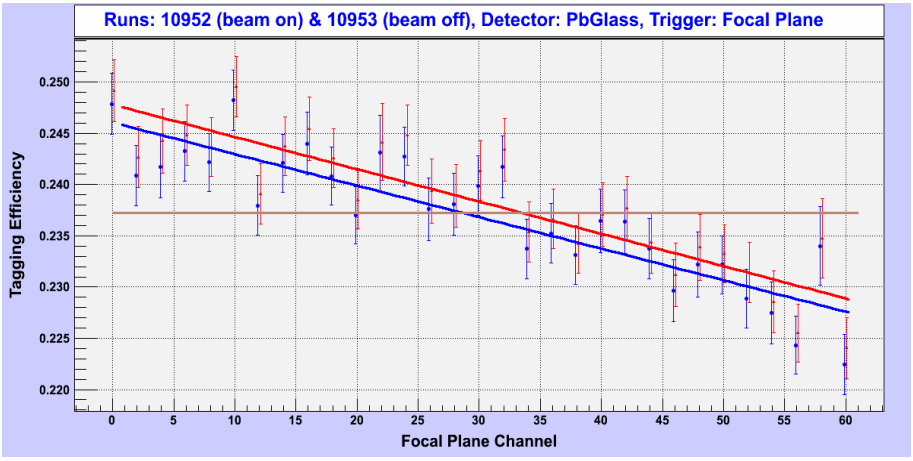

Figure 27: ϵ_{tagg} between 20 ms and 40 ms for the FP OR trigger.

During the experiment, two long runs were performed for each of the triggers. The TiP for the FP OR trigger run (10952) was analyzed by dividing the distribution into time intervals and looking at the tagging efficiency in these intervals. The tagging efficiency using the FP OR trigger in the time interval 20-40 ms is shown in Fig. 27. See Appendix E for a complete set of results.

Channel	20-40 ms	40-60 ms	60-80 ms	80-100 ms
0	0.2466 ± 0.0036	0.2492± 0.0030	0.2422 ± 0.0036	0.2427 ± 0.006
2	0.2424 ± 0.0035	0.2427 ± 0.0030	0.2471 ± 0.0037	0.2497 ± 0.006
4	0.2468 ± 0.0037	0.2443 ± 0.0031	0.2435 ± 0.0038	0.2453 ± 0.006
6	0.2432 ± 0.0034	0.2448 ± 0.0029	0.2423 ± 0.0036	0.2380 ± 0.006
8	0.2436 ± 0.0034	0.2437 ± 0.0029	0.2446 ± 0.0035	0.2393 ± 0.006
10	0.2389 ± 0.0034	0.2496 ± 0.0030	0.2460 ± 0.0036	0.2472 ± 0.006
12	0.2381 ± 0.0034	0.2391 ± 0.0029	0.2385 ± 0.0036	0.2441 ± 0.006
14	0.2367 ± 0.0033	0.2437 ± 0.0029	0.2404 ± 0.0035	0.2363 ± 0.006
16	0.2366 ± 0.0035	0.2454 ± 0.0031	0.2437 ± 0.0037	0.2433 ± 0.006
18	0.2370 ± 0.0034	0.2426 ± 0.0029	0.2422 ± 0.0035	0.2380 ± 0.006
20	0.2383 ± 0.0034	0.2385 ± 0.0028	0.2416 ± 0.0035	0.2417 ± 0.006
22	0.2375 ± 0.0043	0.2442 ± 0.0037	0.2456 ± 0.0046	0.2404 ± 0.008
24	0.2423 ± 0.0034	0.2448 ± 0.0029	0.2394 ± 0.0035	0.2453 ± 0.006
26	0.2414 ± 0.0037	0.2394 ± 0.0031	0.2414 ± 0.0038	0.2342 ± 0.006
28	0.2416 ± 0.0036	0.2389 ± 0.0031	0.2413 ± 0.0038	0.2413 ± 0.006
30	0.2355 ± 0.0034	0.2414 ± 0.0029	0.2377 ± 0.0035	0.2363 ± 0.006
32	0.2408 ± 0.0035	0.2434 ± 0.0030	0.2390 ± 0.0037	0.2370 ± 0.006
34	0.2379 ± 0.0035	0.2354 ± 0.0029	0.2371 ± 0.0036	0.2316 ± 0.006
36	0.2401 ± 0.0035	0.2366 ± 0.0029	0.2294 ± 0.0035	0.2293 ± 0.006
38	0.2305 ± 0.0033	0.2342 ± 0.0029	0.2349 ± 0.0035	0.2278 ± 0.006
40	0.2366 ± 0.0036	0.2371 ± 0.0031	0.2290 ± 0.0037	0.2365 ± 0.006
42	0.2298 ± 0.0036	0.2377 ± 0.0031	0.2368 ± 0.0038	0.2418 ± 0.006
44	0.2276 ± 0.0034	0.2343 ± 0.0030	0.2368± 0.0037	0.2291 ± 0.006
46	0.2297 ± 0.0036	0.2312 ± 0.0031	0.2311 ± 0.0038	0.2244 ± 0.006
48	0.2412 ± 0.0038	0.2339 ± 0.0032	0.2298 ± 0.0039	0.2406 ± 0.007
50	0.2318 ± 0.0034	0.2333 ± 0.0028	0.2261 ± 0.0034	0.2220 ± 0.006
52	0.2316 ± 0.0035	0.2314 ± 0.0029	0.2275 ± 0.0036	0.2265 ± 0.006
54	0.2253 ± 0.0036	0.2286 ± 0.0030	0.2307 ± 0.0037	0.2244 ± 0.006
56	0.2226 ± 0.0033	0.2255 ± 0.0028	0.2236 ± 0.0035	0.2244 ± 0.006
58	0.2344 ± 0.0046	0.2347 ± 0.0039	0.2312 ± 0.0047	0.2404 ± 0.008
60	0.2203 ± 0.0035	0.2240 ± 0.0030	0.2214 ± 0.0036	0.2219 ± 0.006

Table 3: Tagging efficiency for the FP channels in different time intervals.

7 Conclusions

From the results it can be concluded that:

- tagging efficiency is constant as a function of run number.
- tagging efficiency is constant as a function of time-in-pulse.
- the absolute value of the tagging efficiency is known to $\pm 0.6\%$ systematic uncertainty.

8 References

References

[Forsberg, 2010] Forsberg, U. (2010). Tagging Efficiency Measurements at High Intensities. Lund: Department of Physics, Lund University.

[Litwack, 2010] Litwack, M. (2010). MAX-lab May09 Tagging-Efficiency Measurements. Lund: Department of Physics, Lund University.

[Jacobsson, 2009] Jacobsson, D. (2009). Calibration of plastic-scintillator detectors at MAX-lab in preparation for experiments. Lund: Department of Physics, Lund University.

[MAX-lab, 2011] MAX-lab, L. U. (n.d.). MAX Injector. Retrieved 05 22, 2011, from MAXlab: `http://www.maxlab.lu.se/maxlab/about/max_injector.html`

[Karlsson, 2005] Karlsson, M. (2005). Two-body Photodisintegration of He-3, Lund: Department of Physics, Lund University.

[Morrison, 2006] Morrison, V. R. (2006). THE PHOTODISINTEGRATION OF DEUTERIUM, Calibration of the Lund Photon Tagger. Lund: MAX-lab, Lund University.

A Tagging-Efficiency Comparisons

Comparisons between tagging efficiencies for the FP OR and Pb-glass triggers have been plotted. These are illustrated in this section.

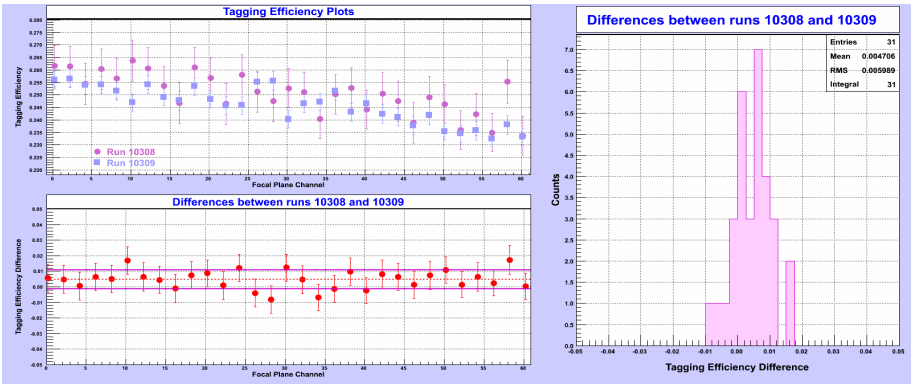

Figure 28: Differences between runs 10308 and 10309.

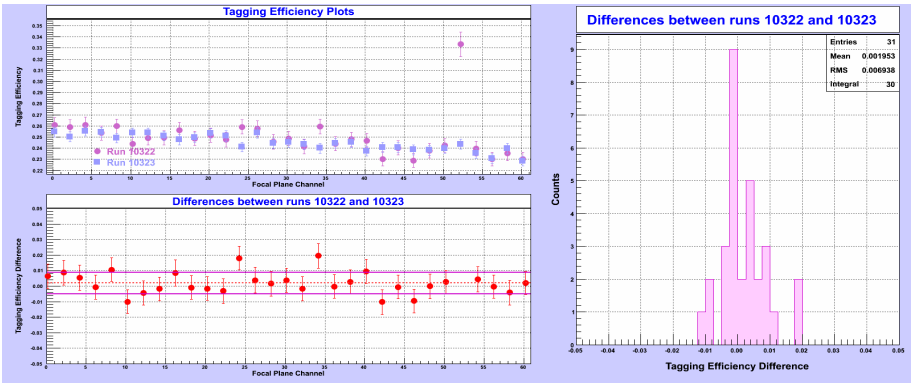

Figure 29: Differences between runs 10322 and 10323.

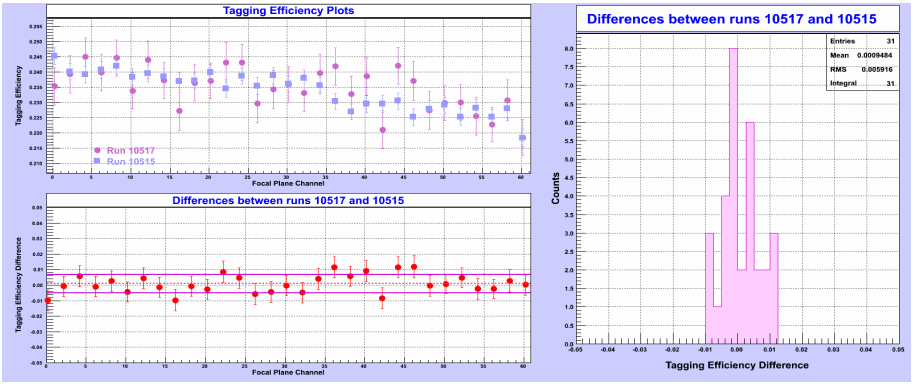

Figure 30: Differences between runs 10517 and 10515.

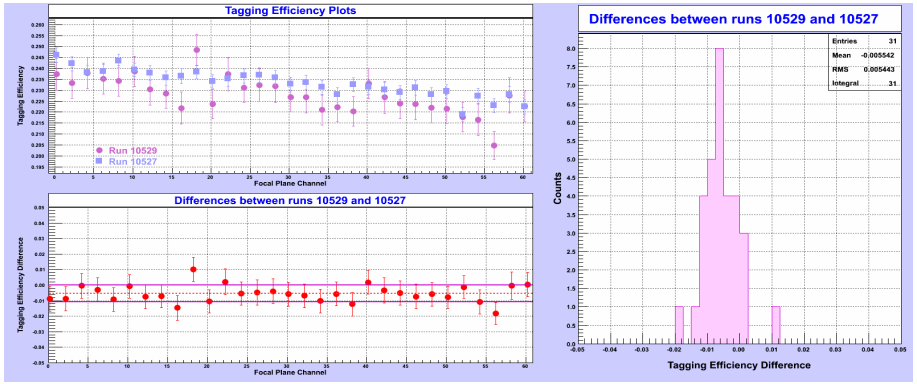

Figure 31: Differences between runs 10529 and 10527.

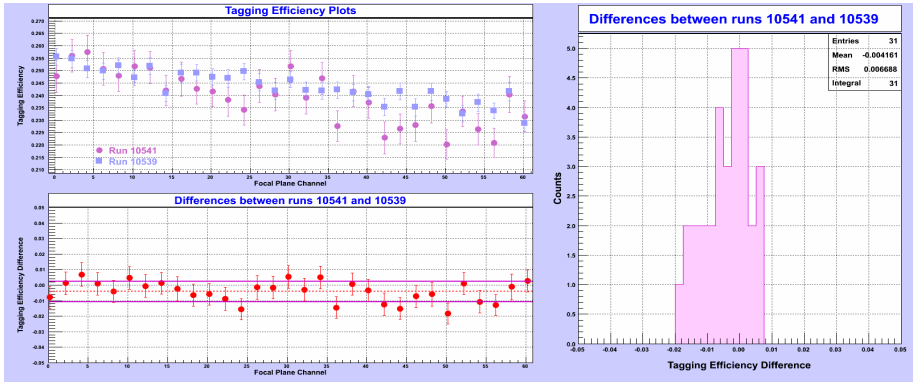

Figure 32: Differences between runs 10541 and 10539.

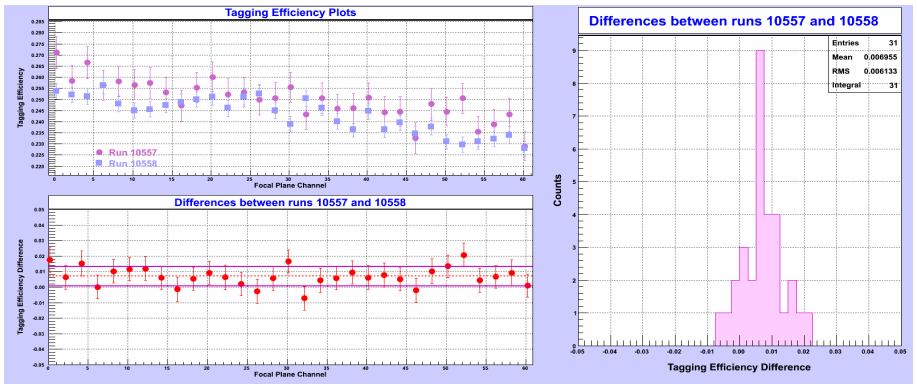

Figure 33: Differences between runs 10557 and 10558.

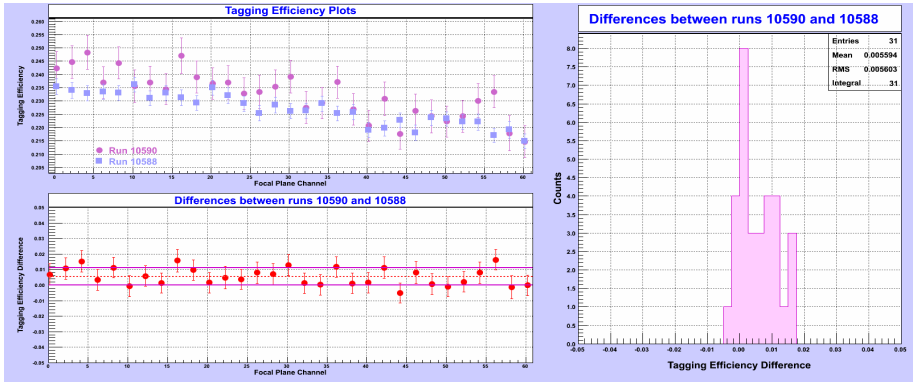

Figure 34: Differences between runs 10590 and 10588.

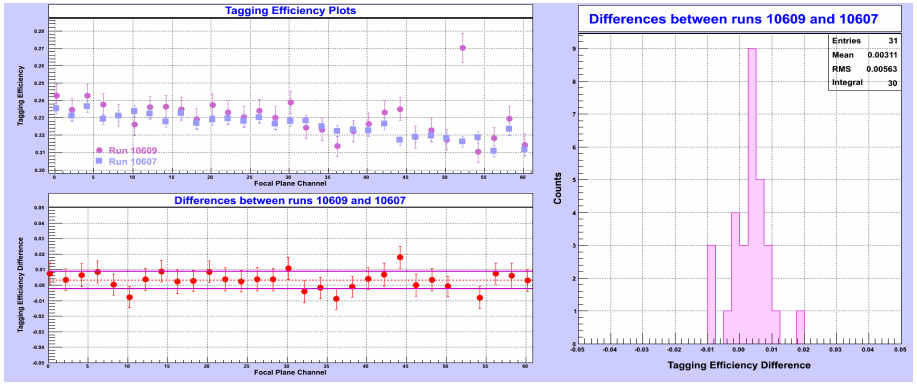

Figure 35: Differences between runs 10609 and 10607.

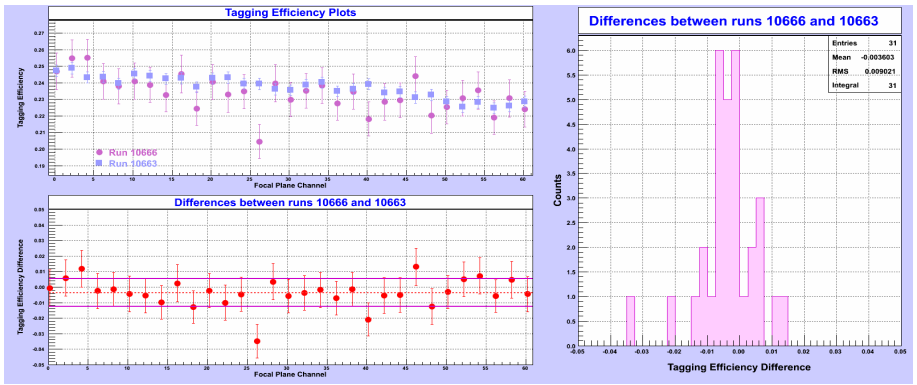

Figure 36: Differences between runs 10666 and 10663.

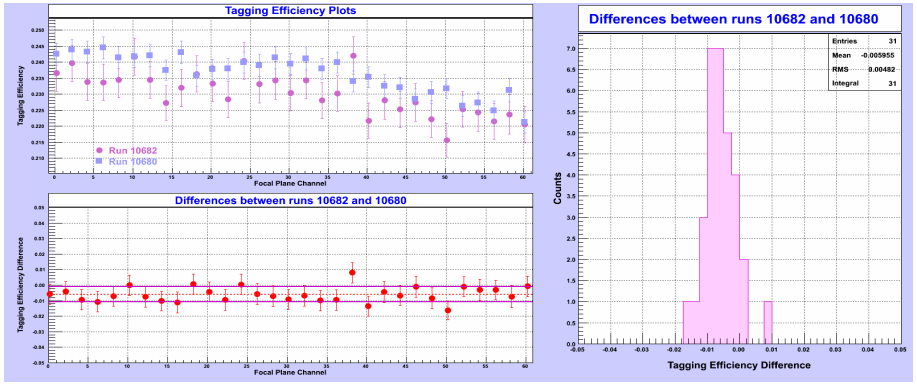

Figure 37: Differences between runs 10682 and 10680.

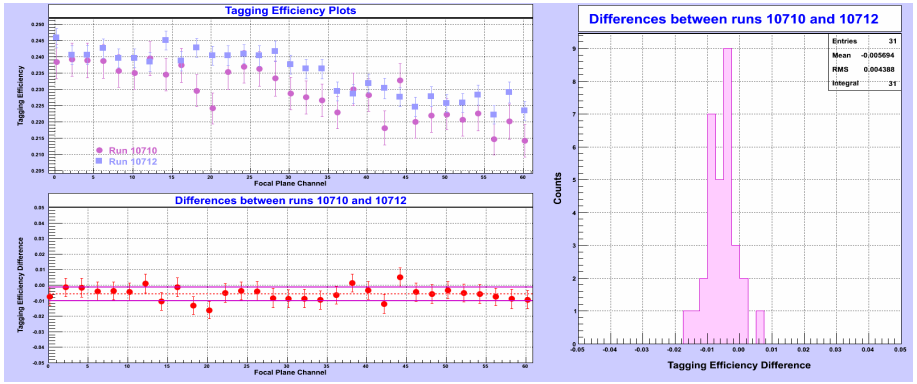

Figure 38: Differences between runs 10710 and 10712.

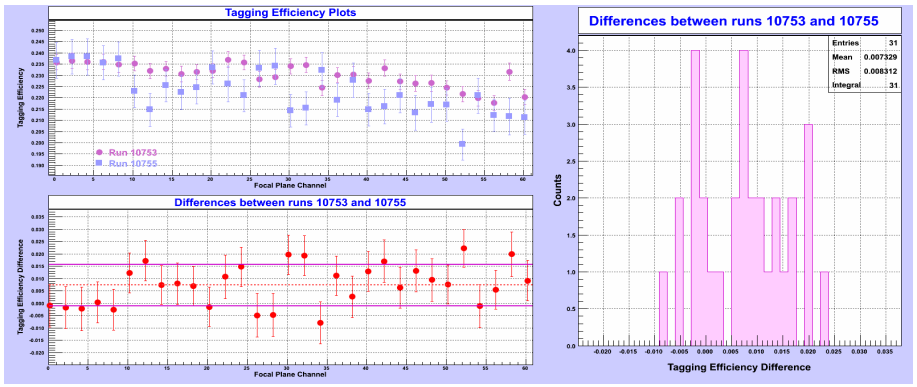

Figure 39: Differences between runs 10753 and 10755.

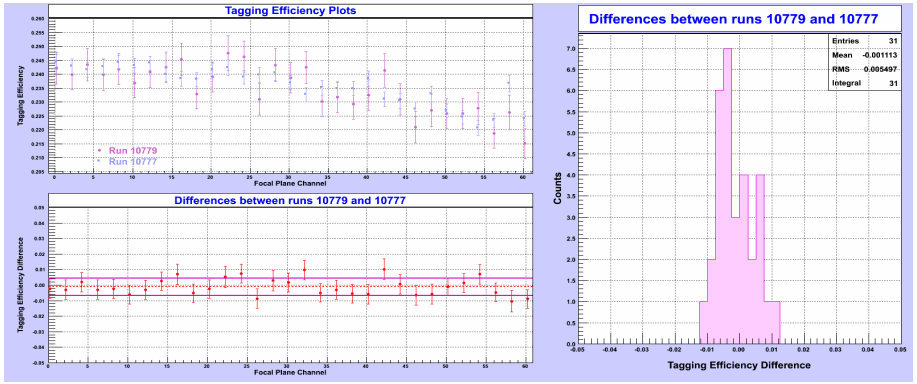

Figure 40: Differences between runs 10779 and 10777.

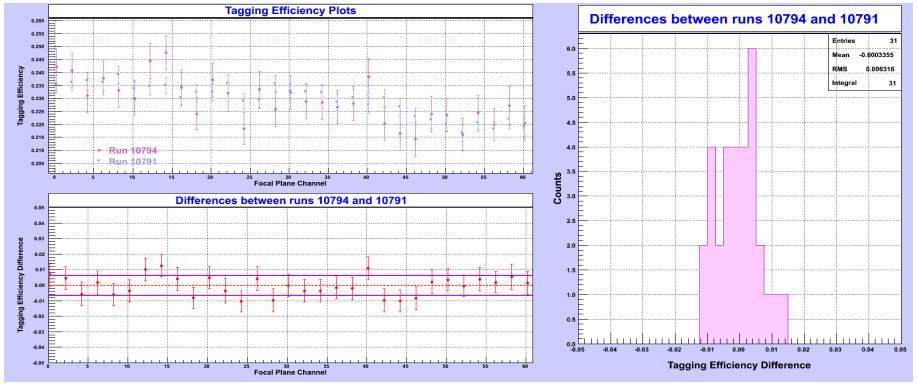

Figure 41: Differences between runs 10794 and 10791.

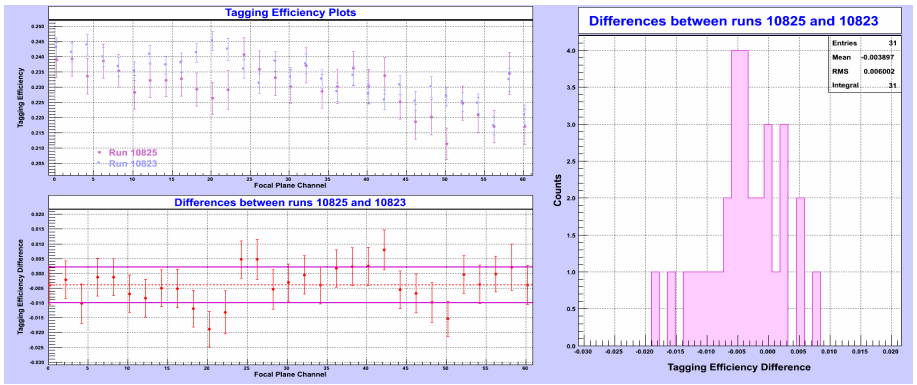

Figure 42: Differences between runs 10825 and 10823.

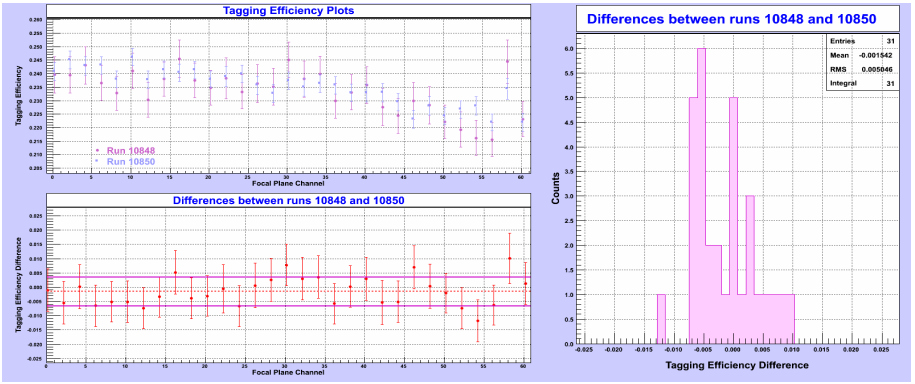

Figure 43: Differences between runs 10848 and 10850.

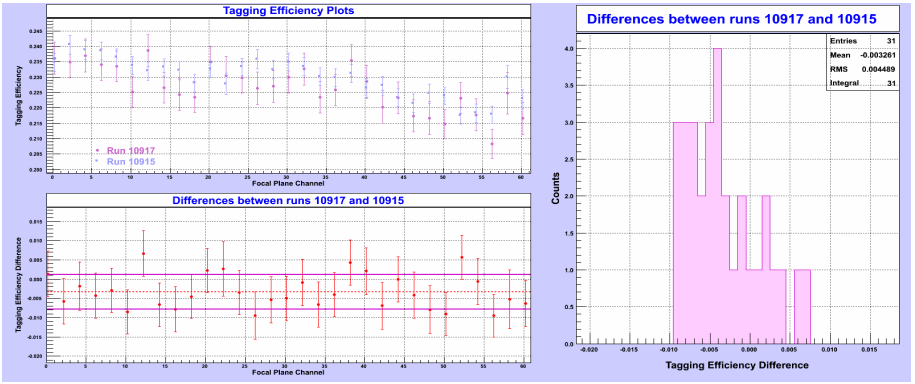

Figure 44: Differences between runs 10917 and 10915.

B FP OR Trigger Tagging-Efficiency Graphs

Tagging efficiencies obtained using the FP OR trigger for each FP channel are presented in this section.

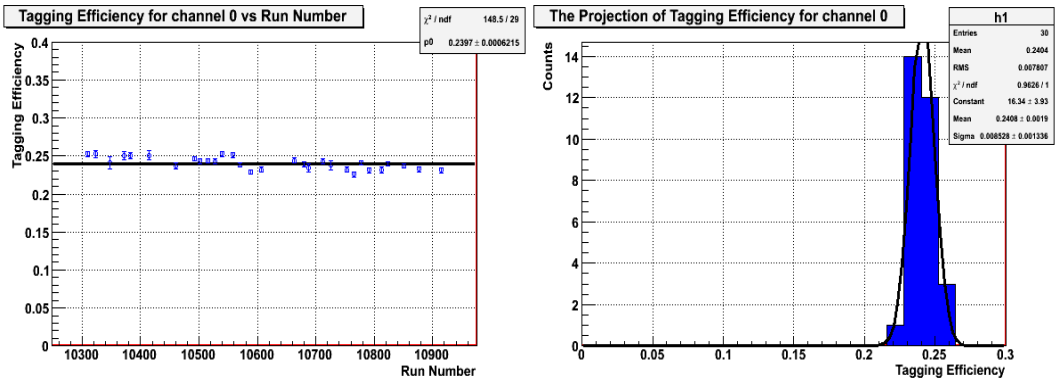

Figure 45: Tagging efficiency plots for FP channel 0.

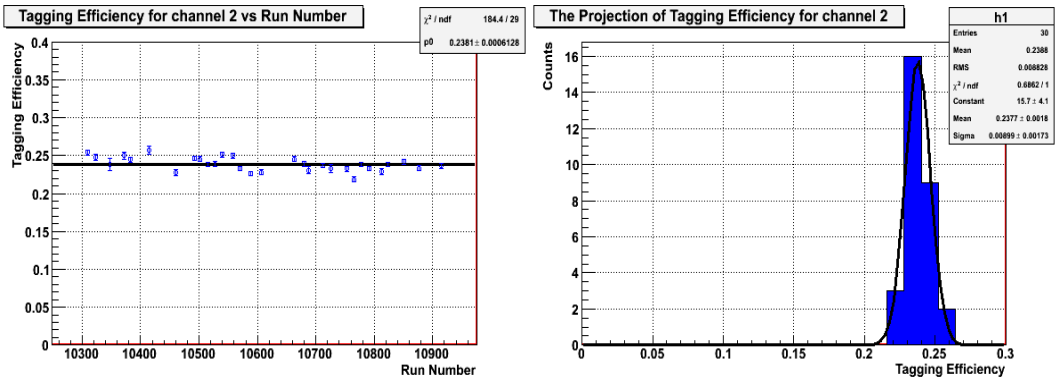

Figure 46: Tagging efficiency plots for FP channel 2.

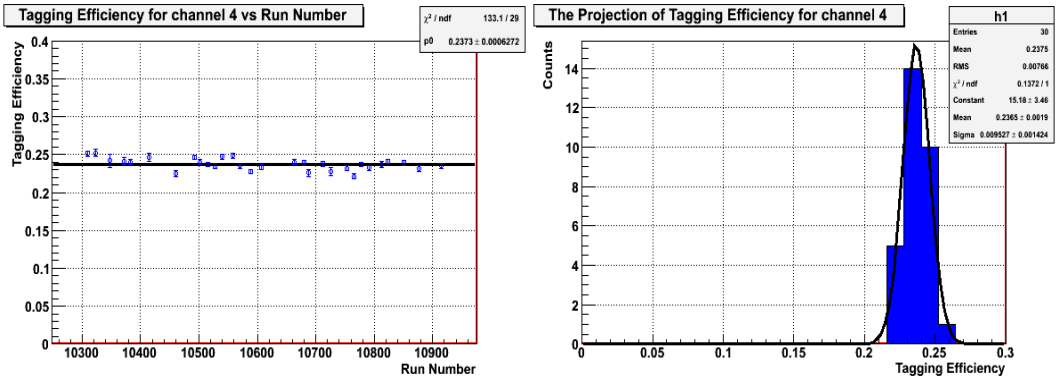

Figure 47: Tagging efficiency plots for FP channel 4.

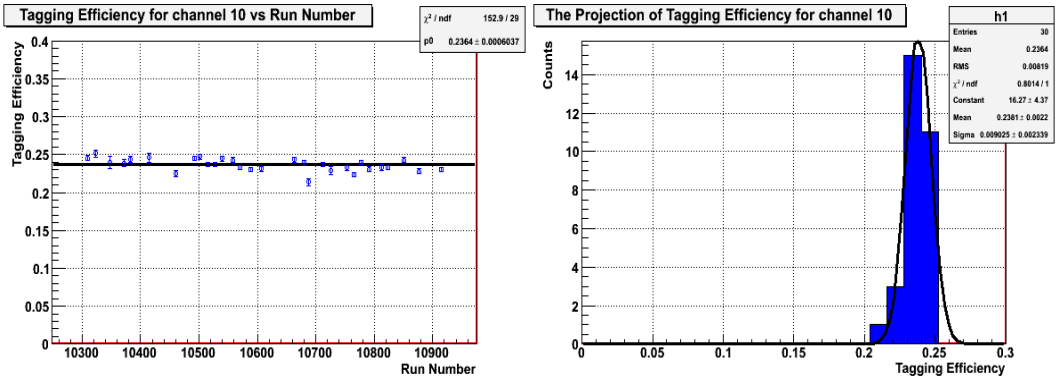

Figure 49: Tagging efficiency plots for FP channel 10.

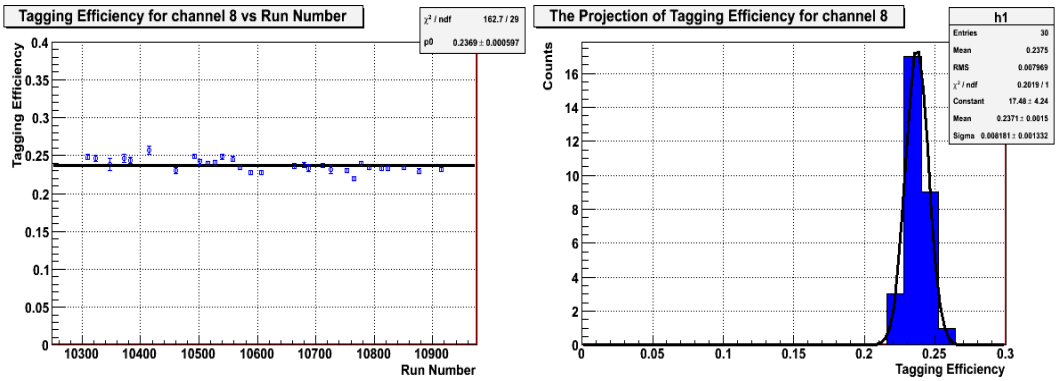

Figure 48: Tagging efficiency plots for FP channel 6.

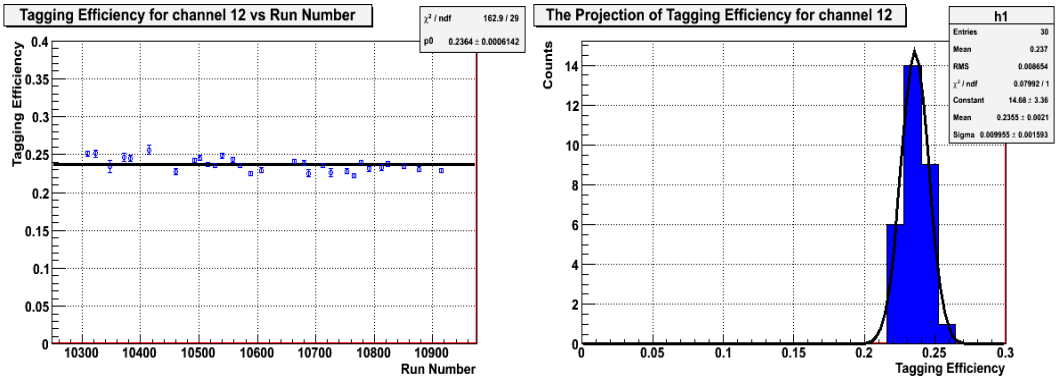

Figure 50: Tagging efficiency plots for FP channel 12.

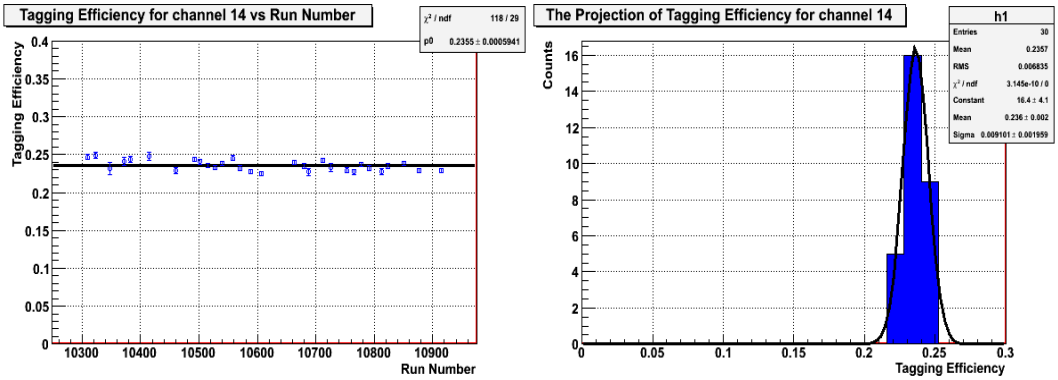

Figure 51: Tagging efficiency plots for FP channel 14.

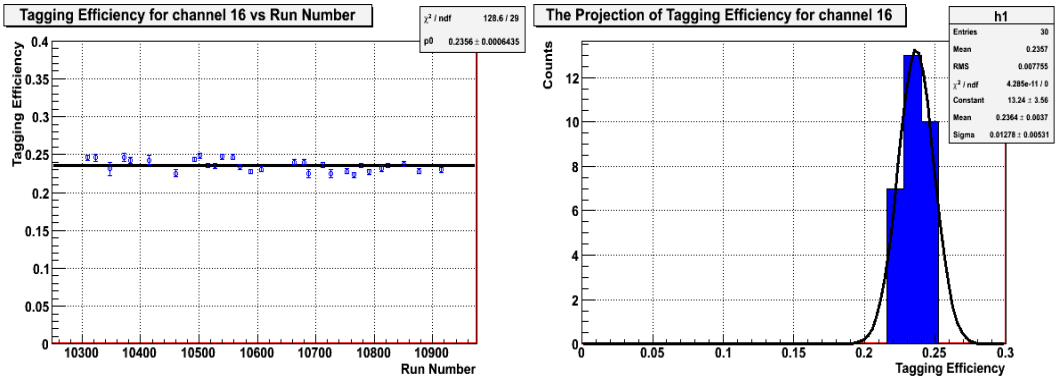

Figure 52: Tagging efficiency plots for FP channel 16.

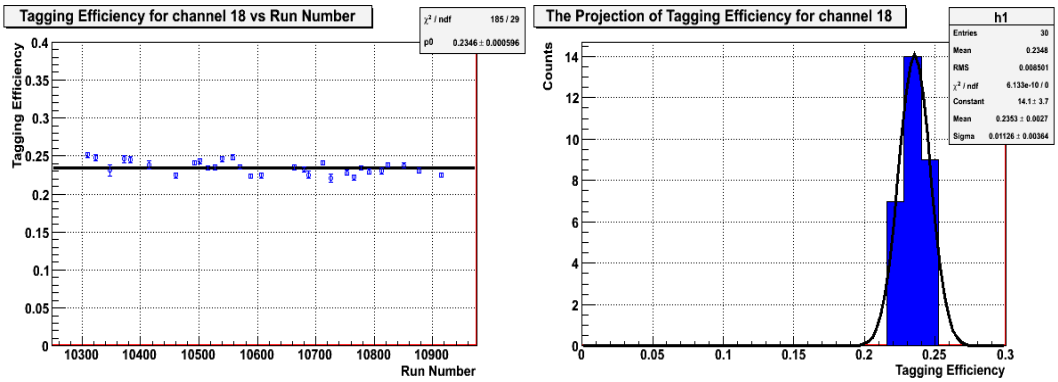

Figure 53: Tagging efficiency plots for FP channel 18.

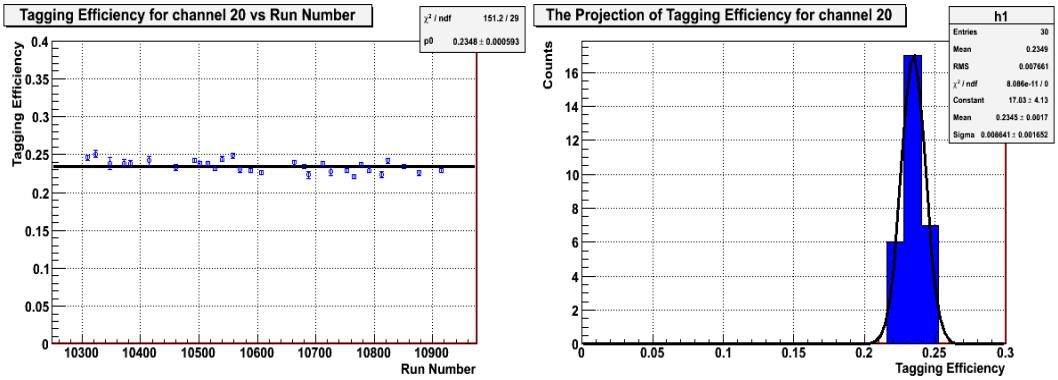

Figure 54: Tagging efficiency plots for FP channel 20.

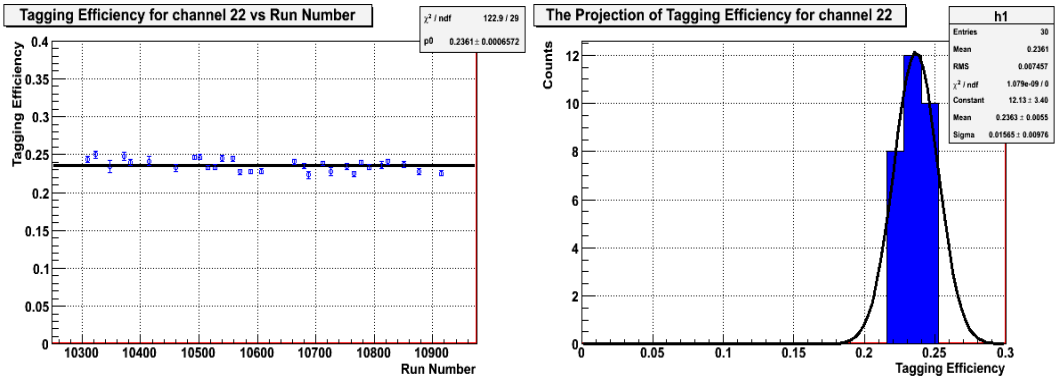

Figure 55: Tagging efficiency plots for FP channel 22.

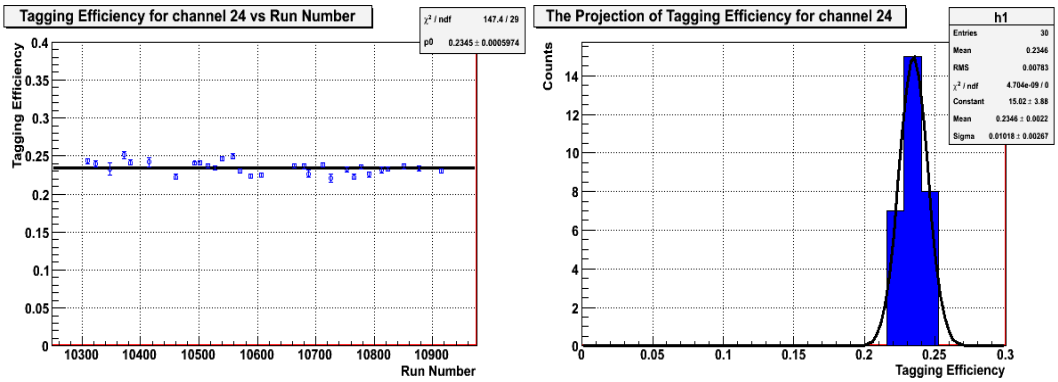

Figure 56: Tagging efficiency plots for FP channel 24.

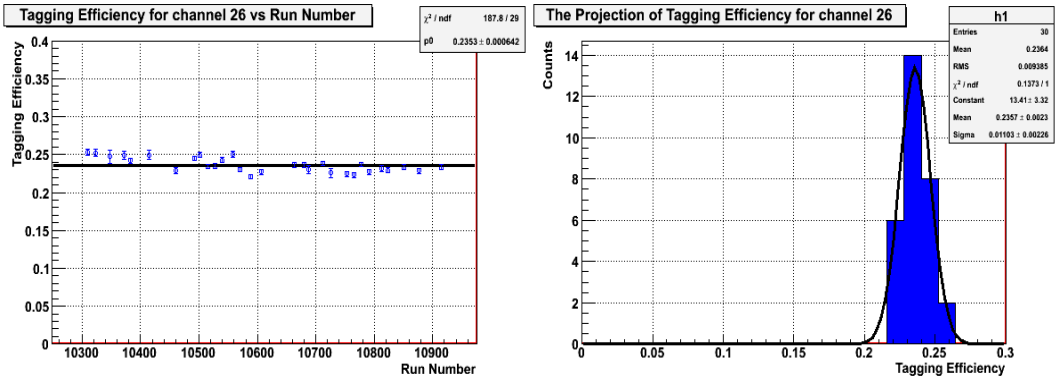

Figure 57: Tagging efficiency plots for FP channel 26.

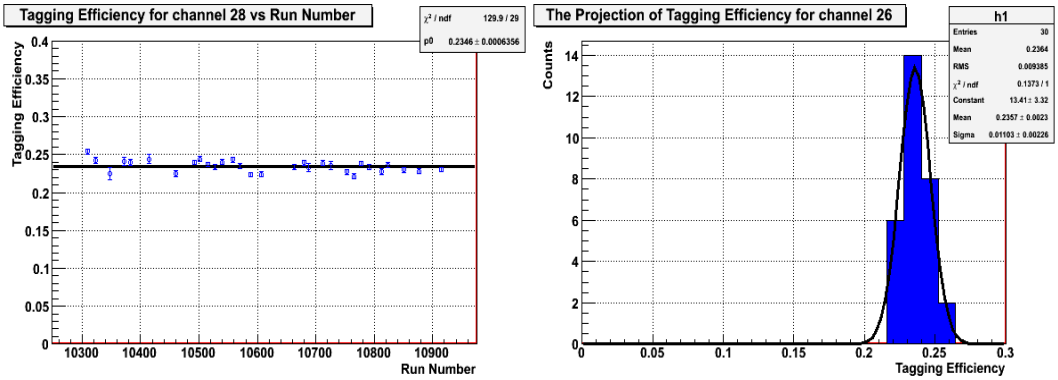

Figure 58: Tagging efficiency plots for FP channel 28.

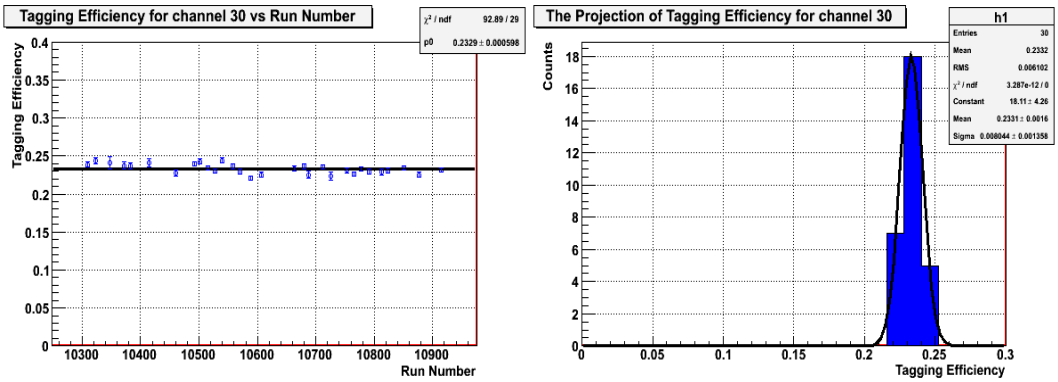

Figure 59: Tagging efficiency plots for FP channel 30.

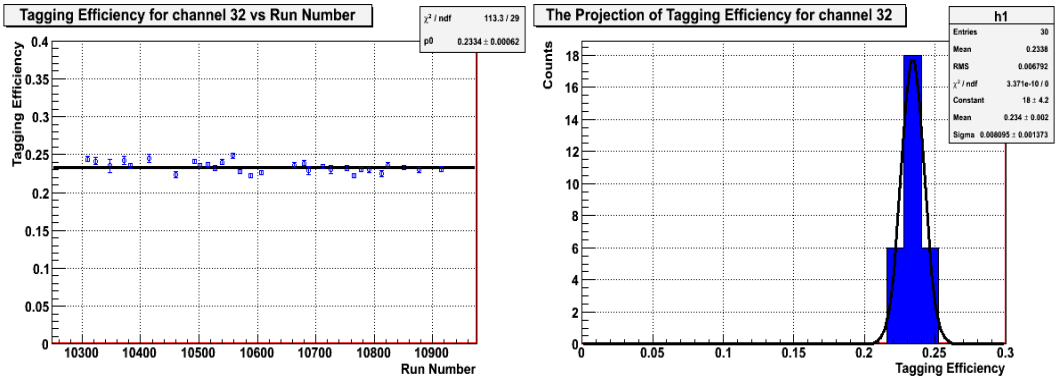

Figure 60: Tagging efficiency plots for FP channel 32.

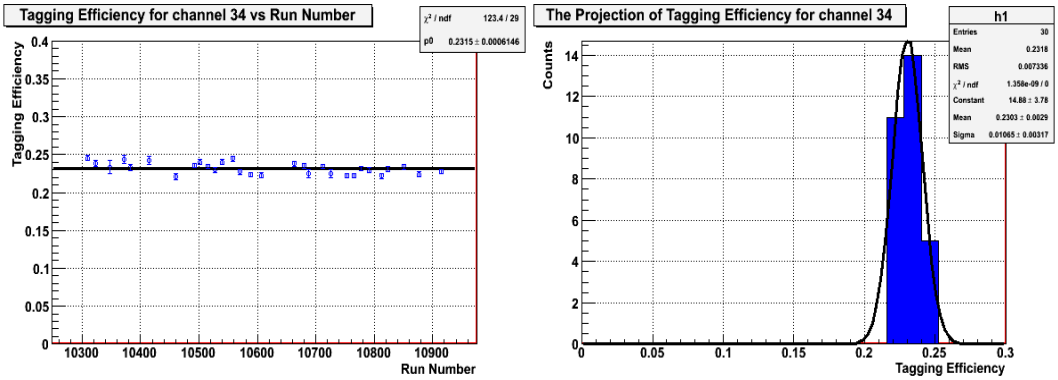

Figure 61: Tagging efficiency plots for FP channel 34.

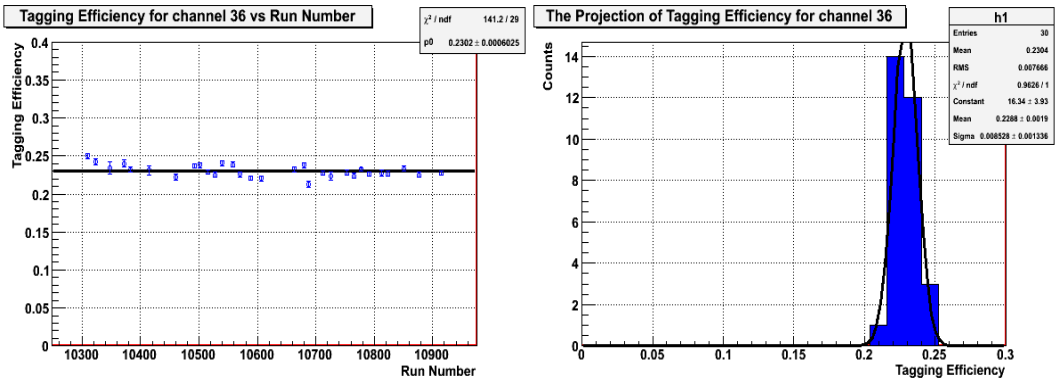

Figure 62: Tagging efficiency plots for FP channel 36.

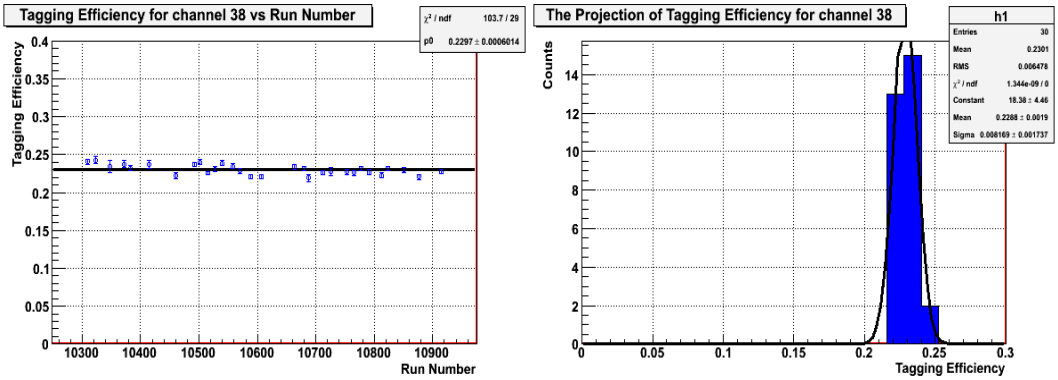

Figure 63: Tagging efficiency plots for FP channel 38.

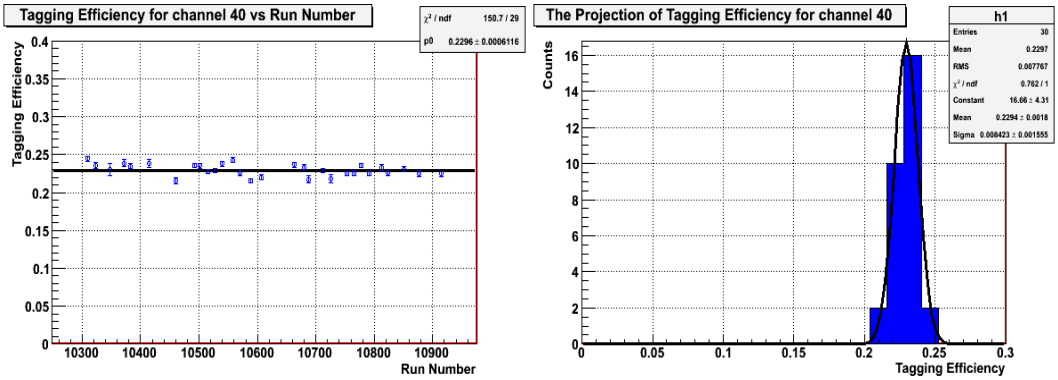

Figure 64: Tagging efficiency plots for FP channel 40.

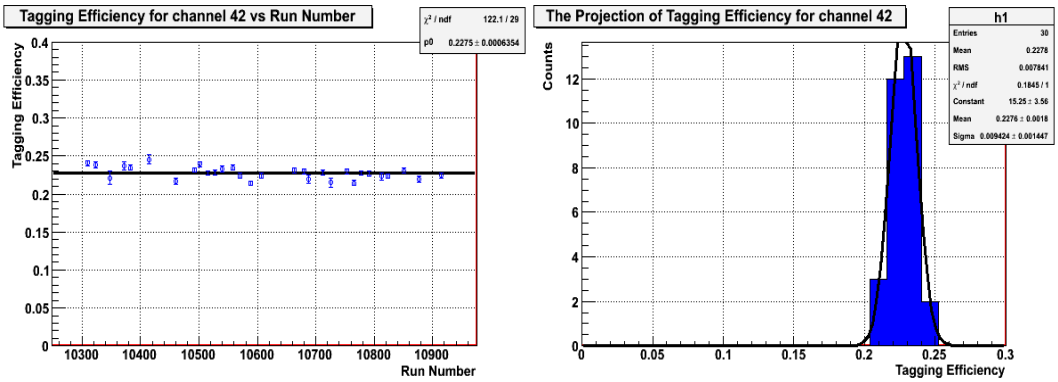

Figure 65: Tagging efficiency plots for FP channel 42.

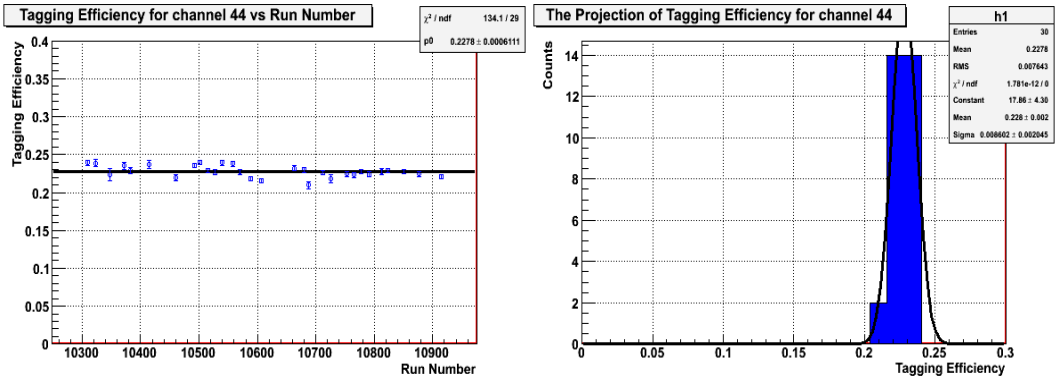

Figure 66: Tagging efficiency plots for FP channel 44.

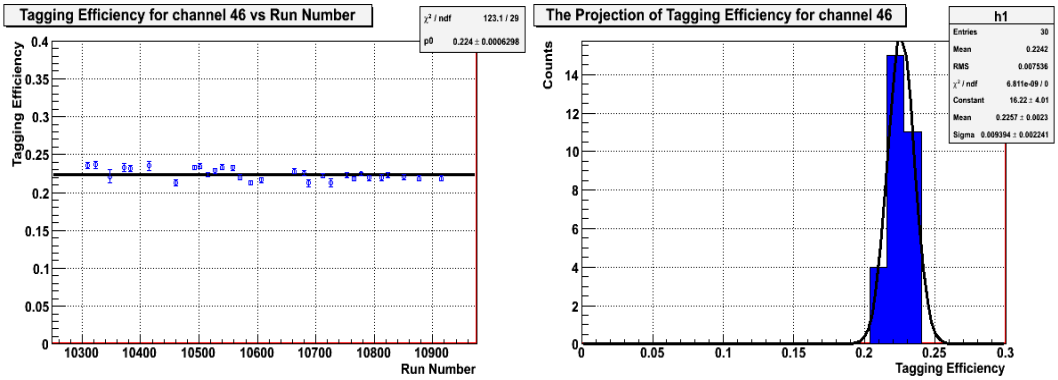

Figure 67: Tagging efficiency plots for FP channel 46.

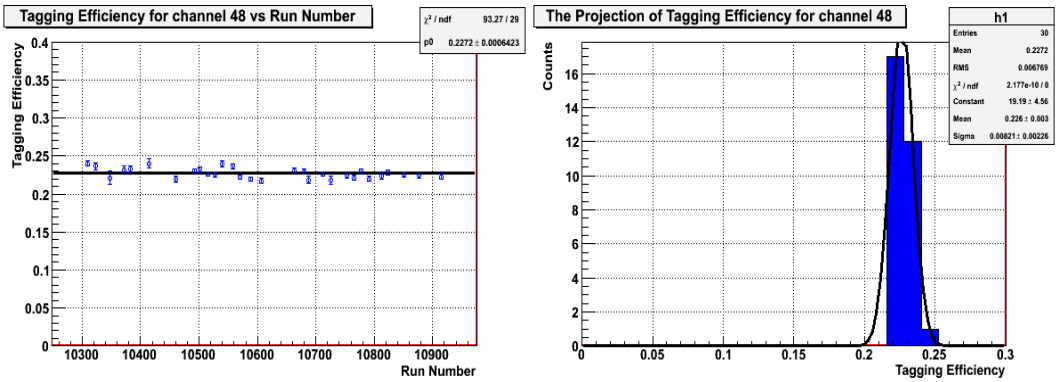

Figure 68: Tagging efficiency plots for FP channel 48.

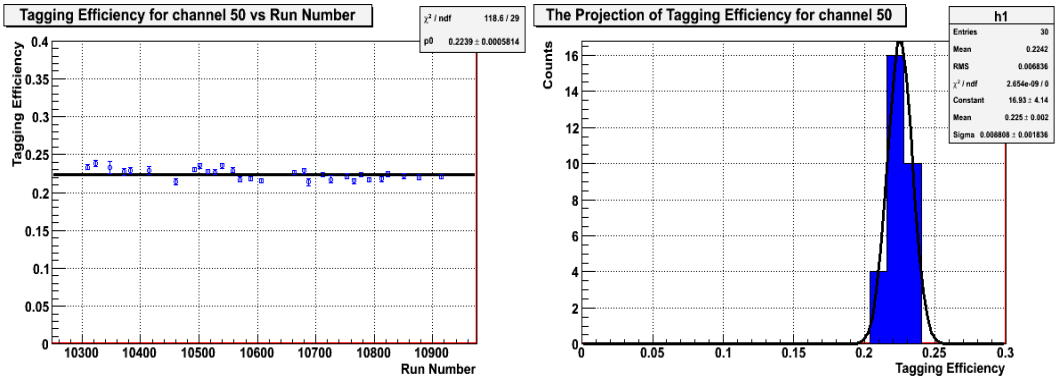

Figure 69: Tagging efficiency plots for FP channel 50.

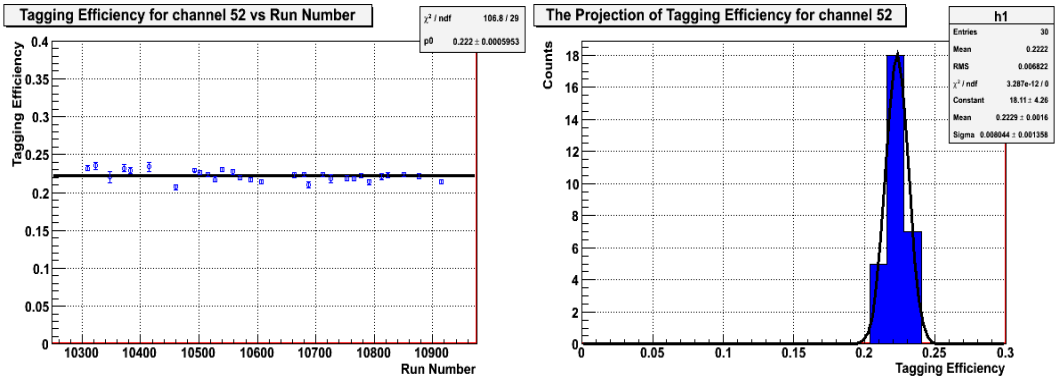

Figure 70: Tagging efficiency plots for FP channel 52.

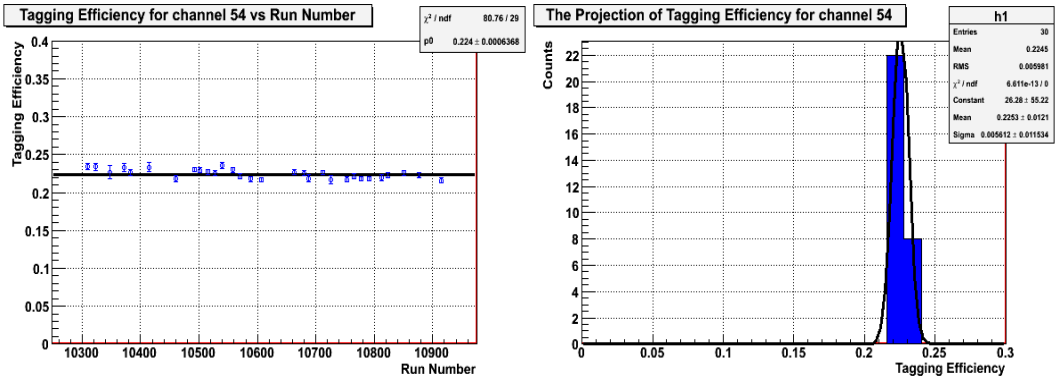

Figure 71: Tagging efficiency plots for FP channel 54.

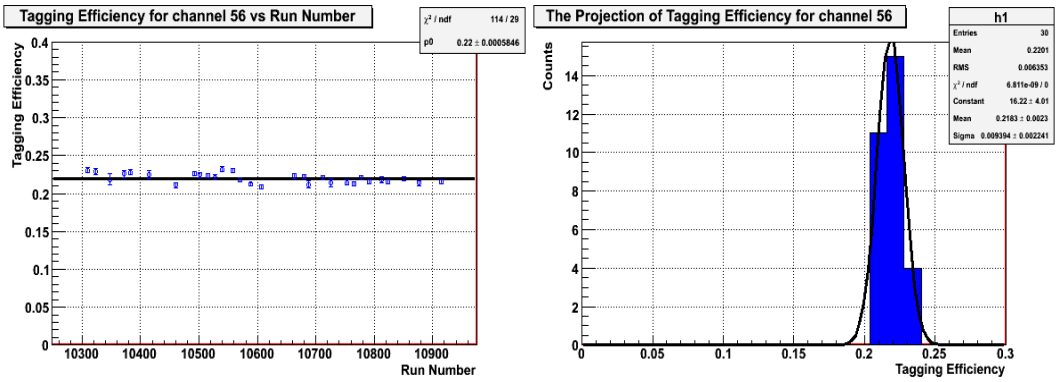

Figure 72: Tagging efiiciency plots for FP channel 56.

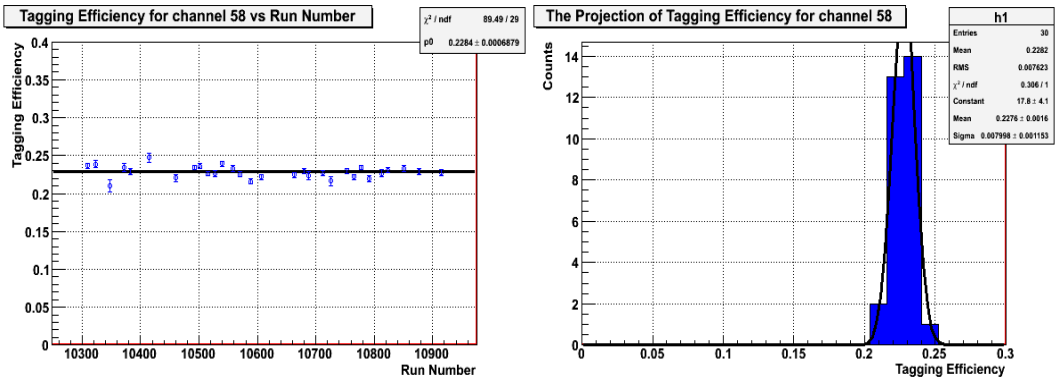

Figure 73: Tagging efficiency plots for FP channel 58.

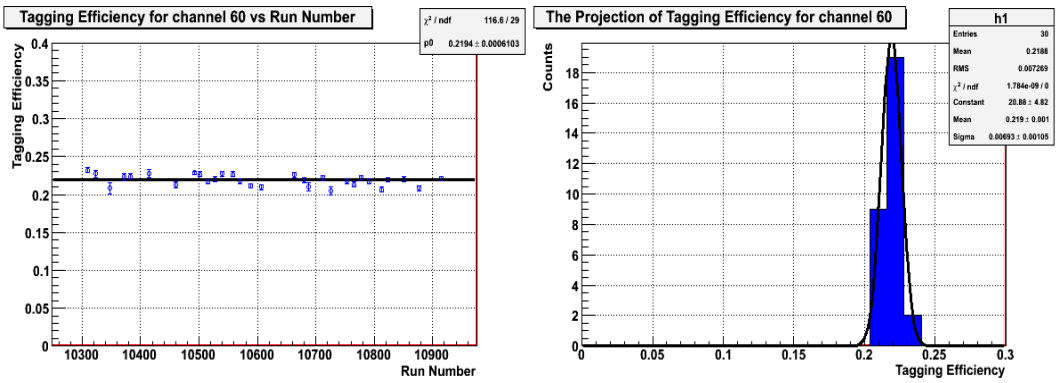

Figure 74: Tagging efficiency plots for FP channel 60.

C Pb-glass Trigger Tagging Efficiency Graphs

Tagging efficiencies obtained using the Pb-glass trigger for each FP channel are presented in this section.

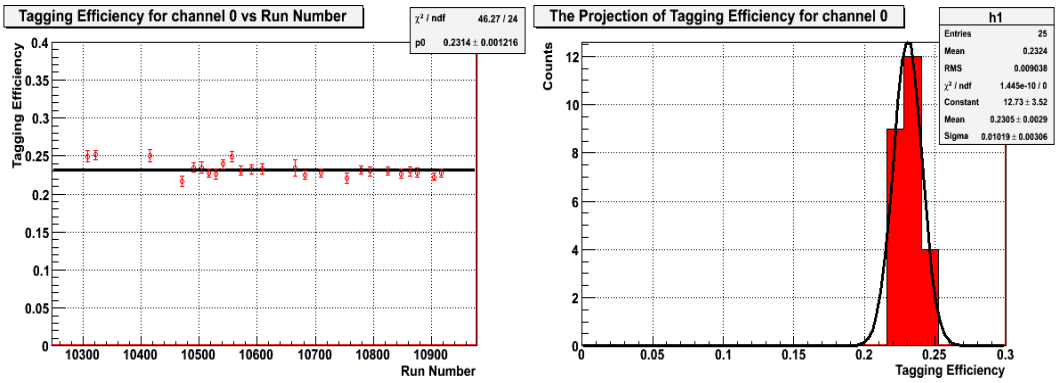

Figure 75: Tagging efficiency plots for FP channel 0.

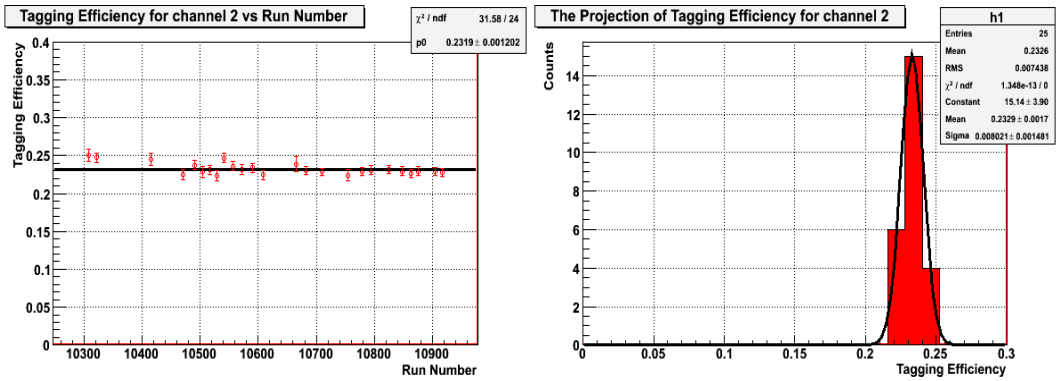

Figure 76: Tagging efficiency plots for FP channel 2.

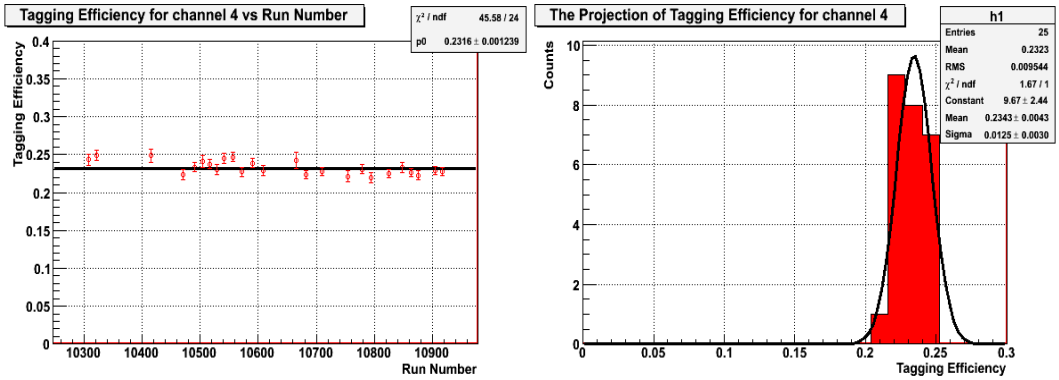

Figure 77: Tagging efficiency plots for FP channel 4.

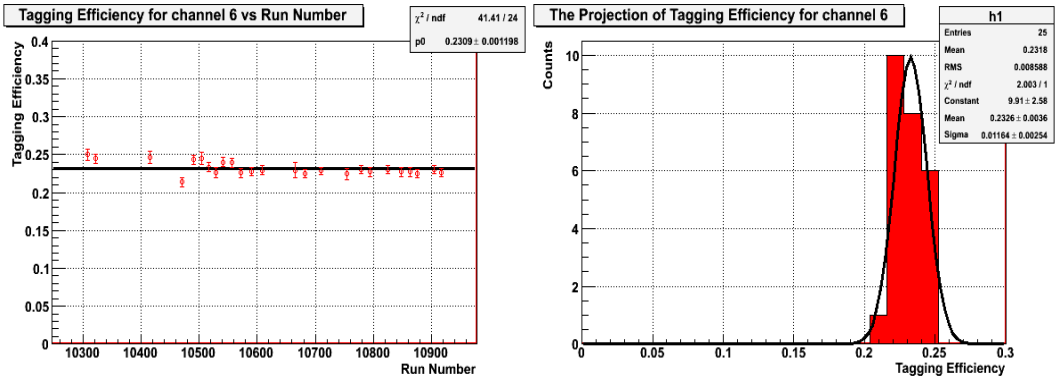

Figure 78: Tagging efficiency plots for FP channel 6.

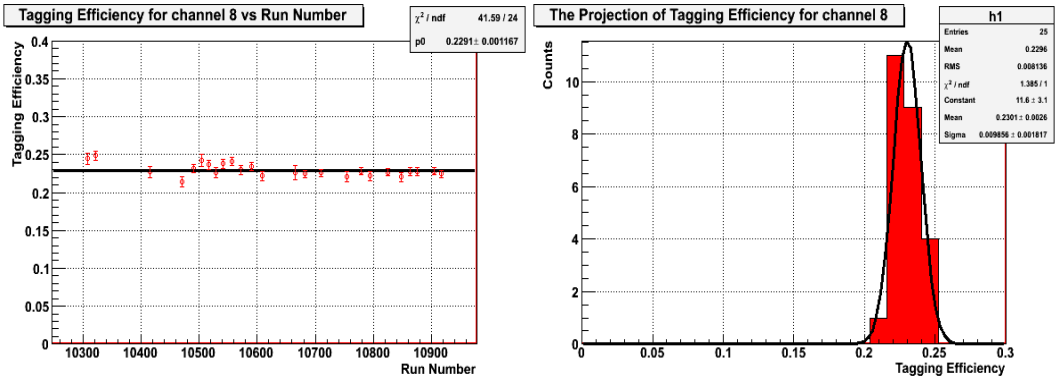

Figure 79: Tagging efficiency plots for FP channel 8.

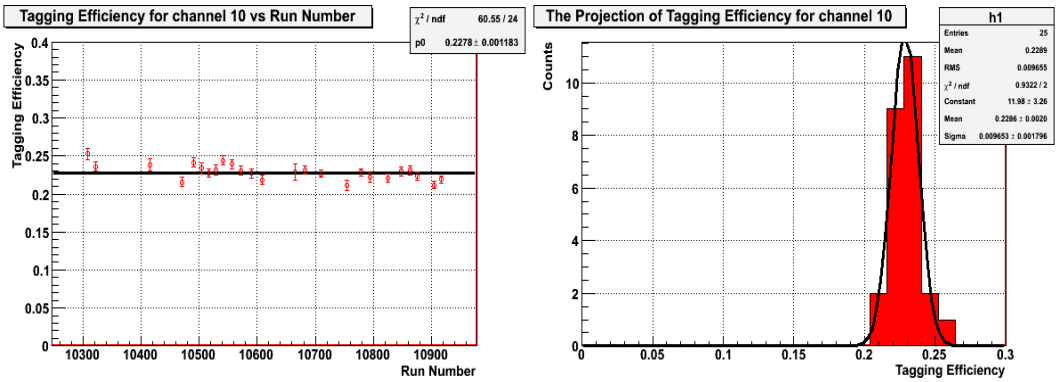

Figure 80: Tagging efficiency plots for FP channel 10.

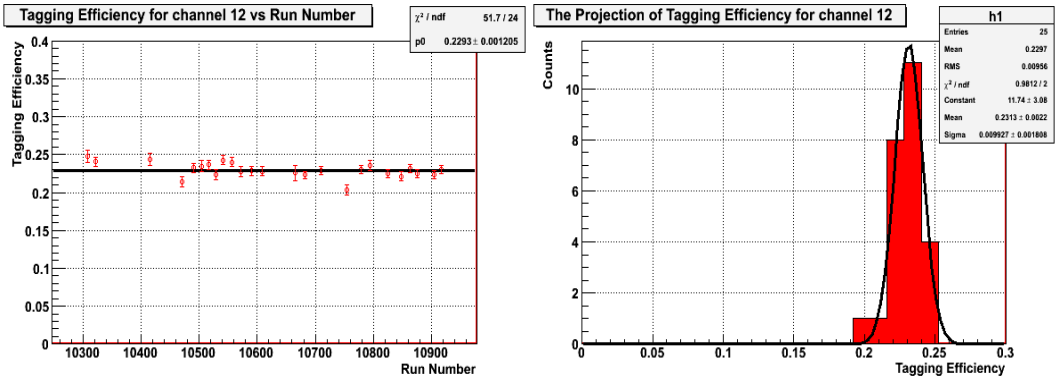

Figure 81: Tagging efficiency plots for FP channel 12.

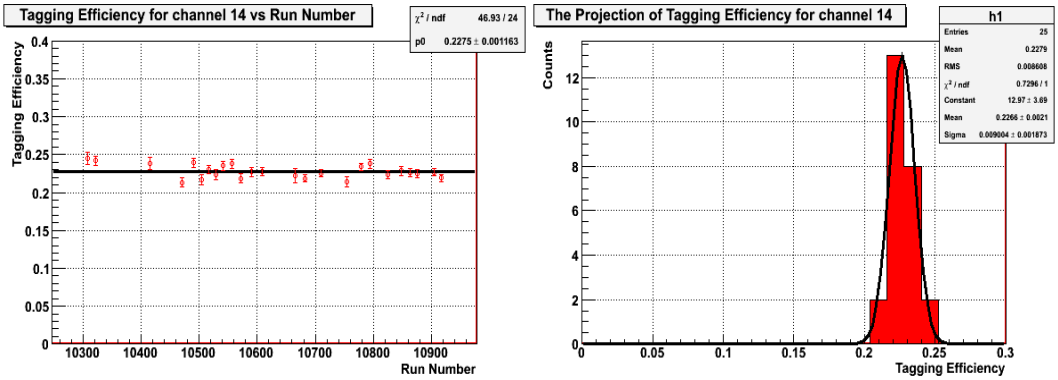

Figure 82: Tagging efficiency plots for FP channel 14.

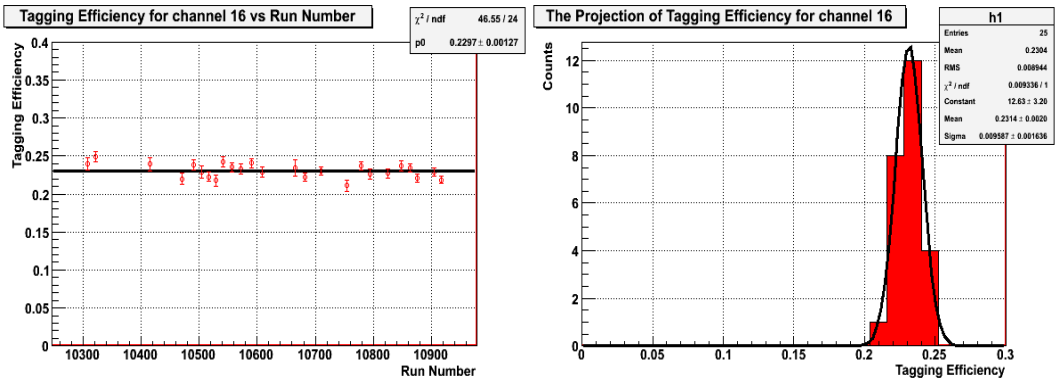

Figure 83: Tagging efficiency plots for FP channel 16.

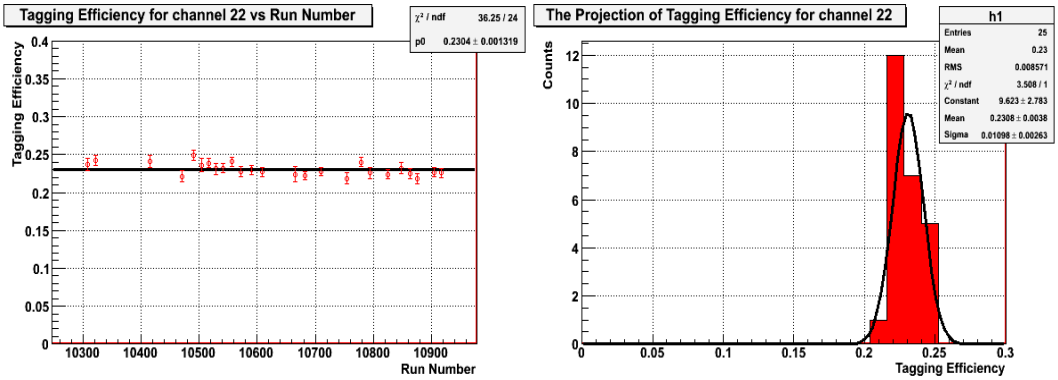

Figure 86: Tagging efficiency plots for FP channel 22.

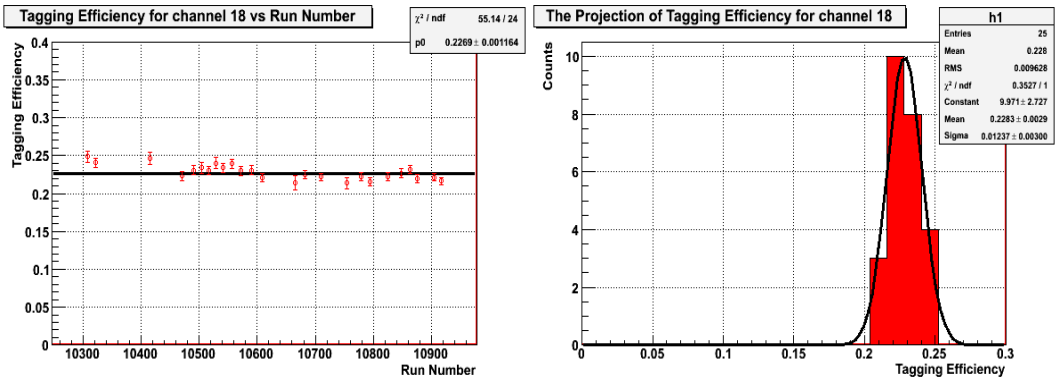

Figure 84: Tagging efficiency plots for FP channel 18.

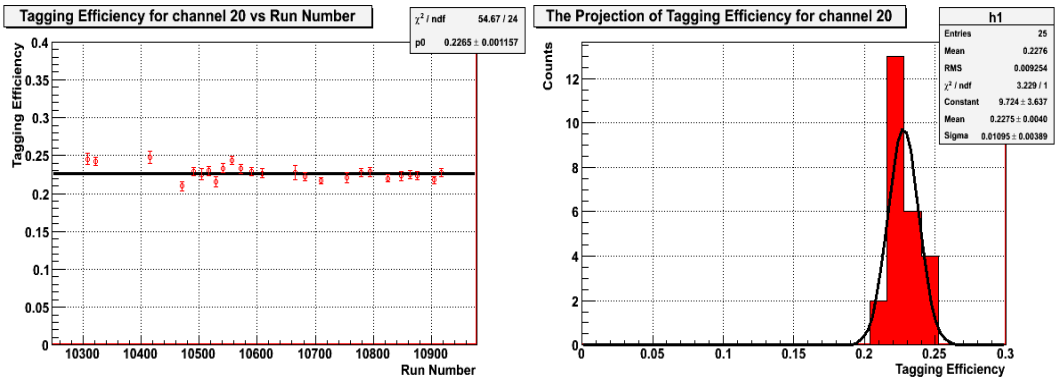

Figure 85: Tagging efficiency plots for FP channel 20.

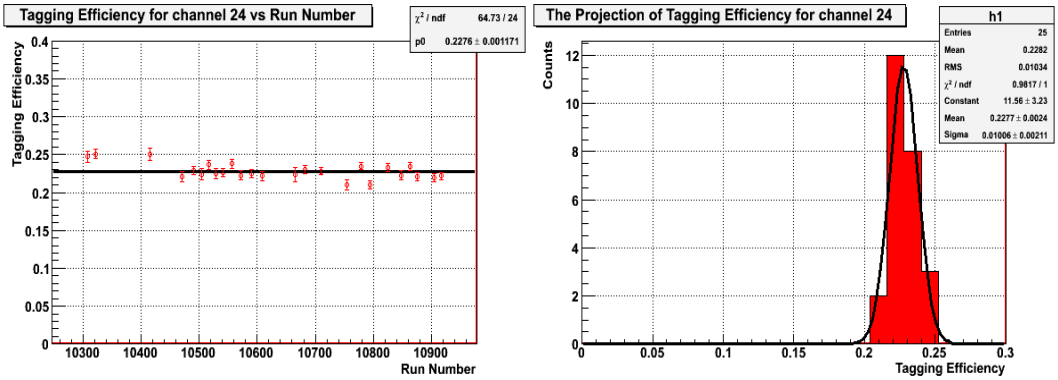

Figure 87: Tagging efficiency plots for FP channel 24.

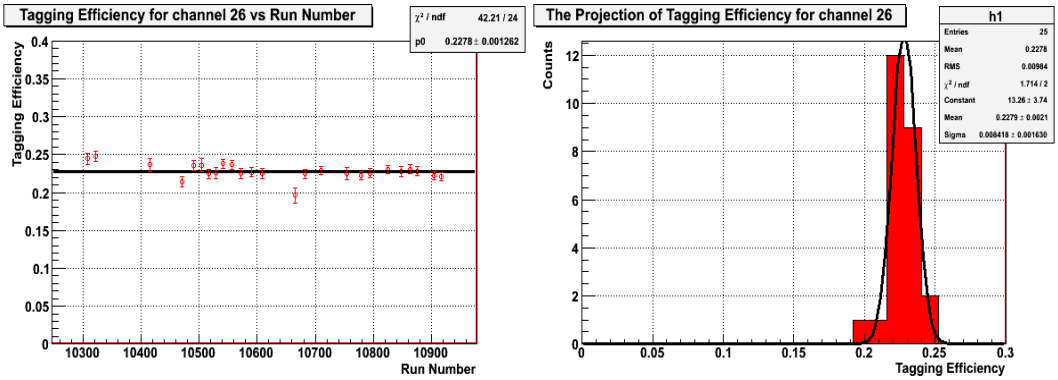

Figure 88: Tagging efficiency plots for FP channel 26.

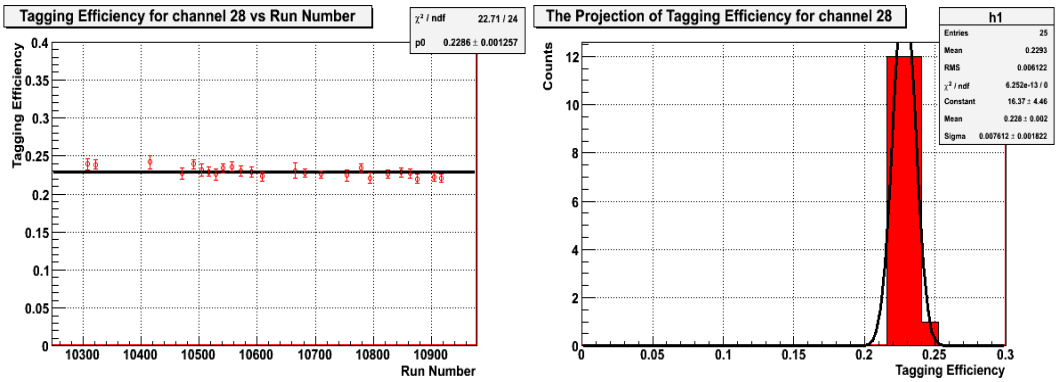

Figure 89: Tagging efficiency plots for FP channel 28.

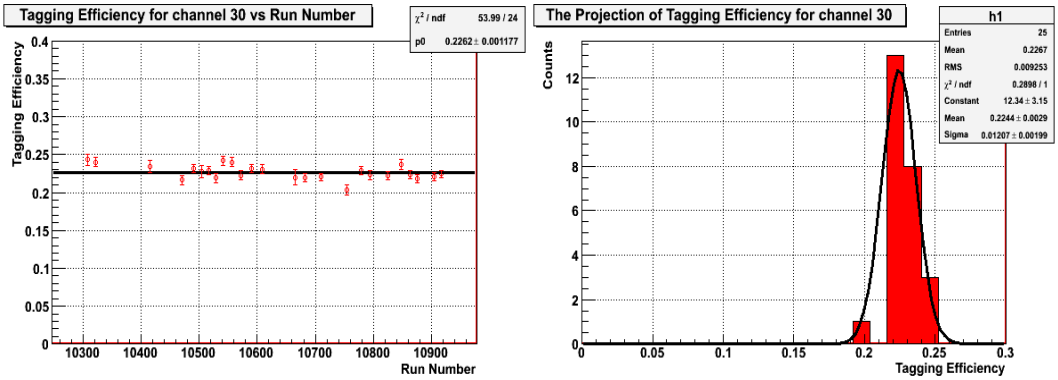

Figure 90: Tagging efficiency plots for FP channel 30.

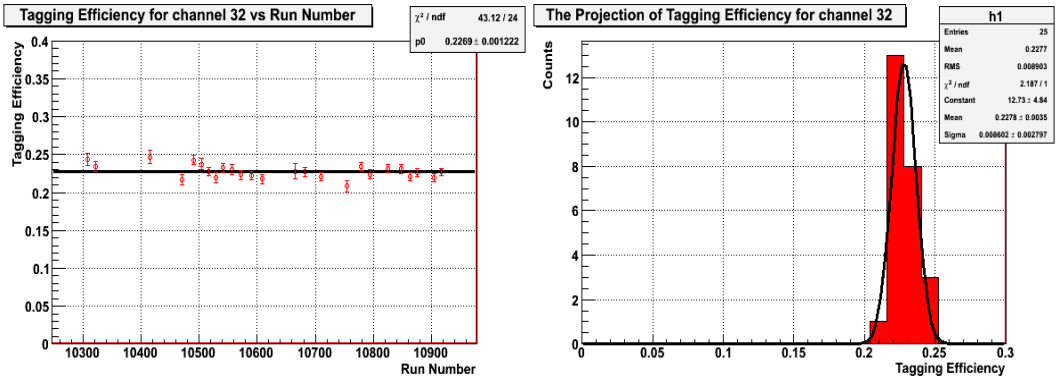

Figure 91: Tagging efficiency plots for FP channel 32.

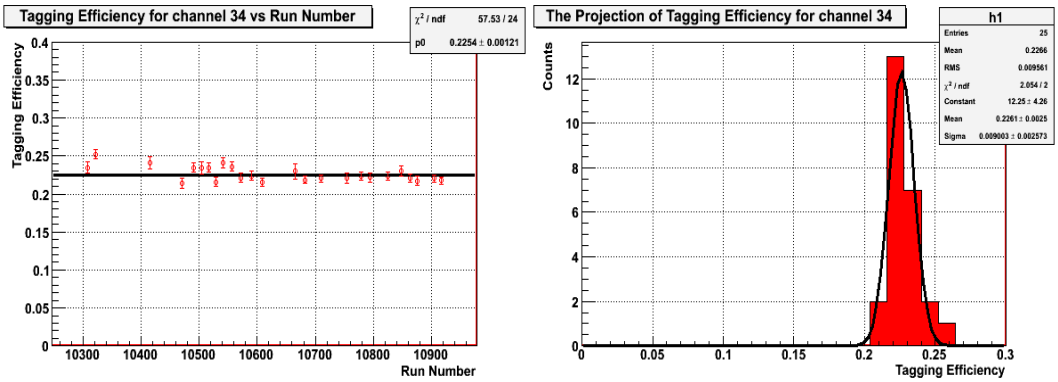

Figure 92: Tagging efficiency plots for FP channel 34.

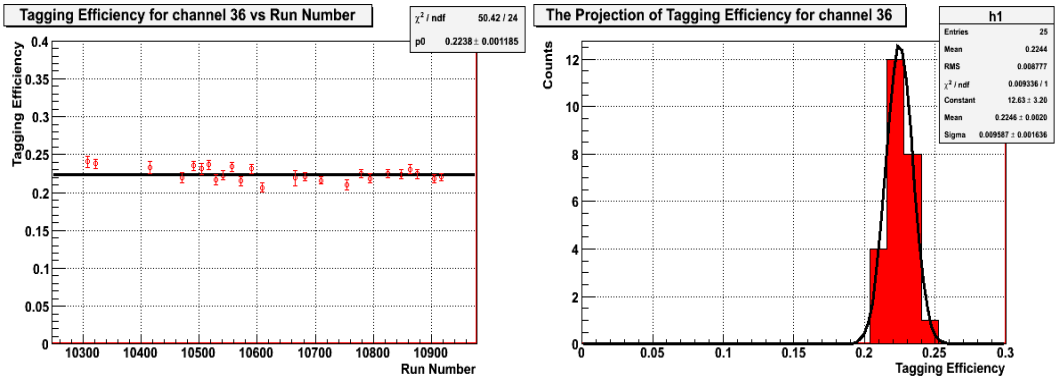

Figure 93: Tagging efficiency plots for FP channel 36.

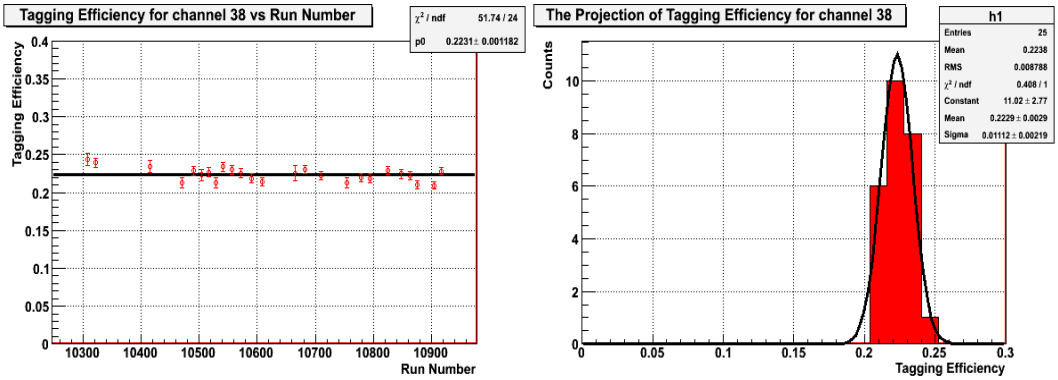

Figure 94: Tagging efficiency plots for FP channel 38.

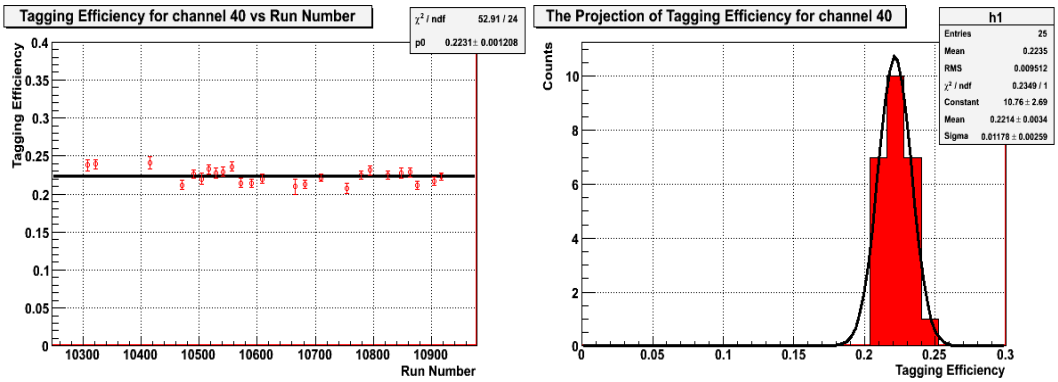

Figure 95: Tagging efficiency plots for FP channel 40.

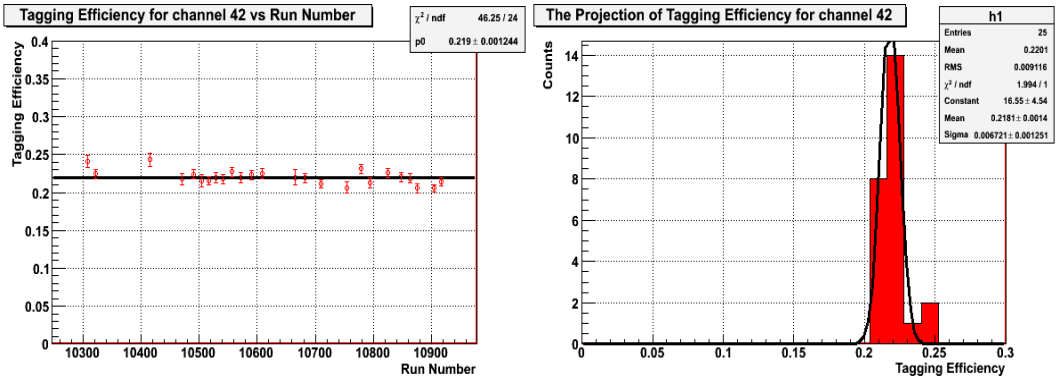

Figure 96: Tagging efficiency plots for FP channel 42.

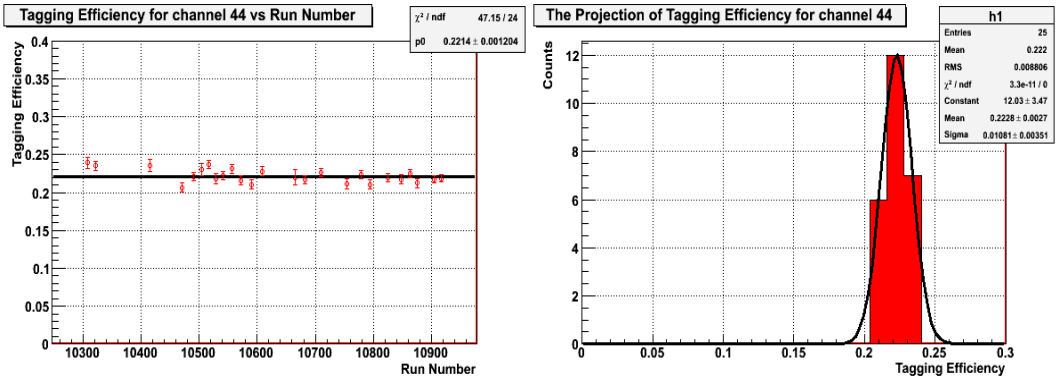

Figure 97: Tagging efficiency plots for FP channel 44.

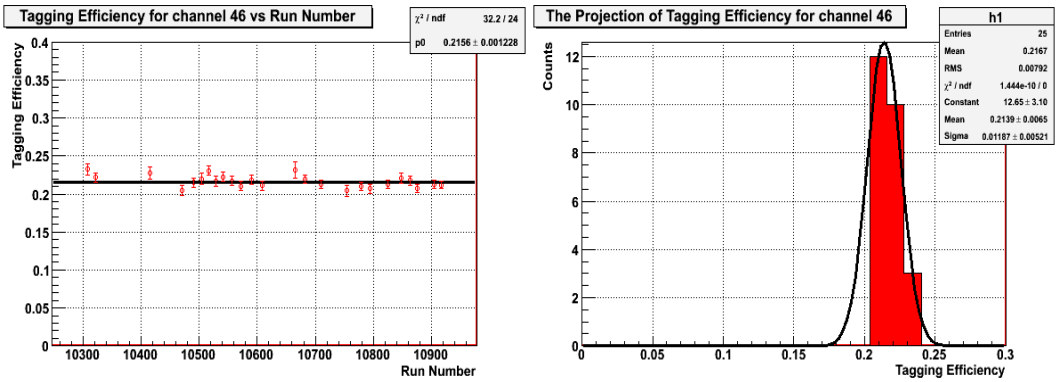

Figure 98: Tagging efficiency plots for FP channel 46.

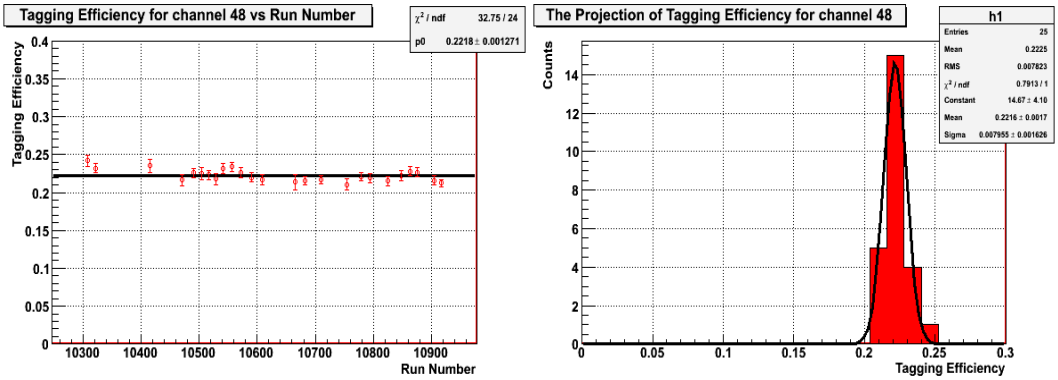

Figure 99: Tagging efficiency plots for FP channel 48.

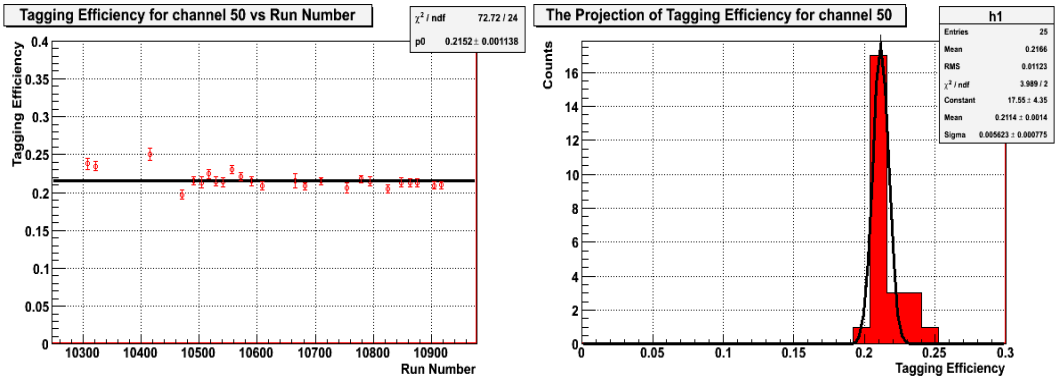

Figure 100: Tagging efficiency plots for FP channel 50.

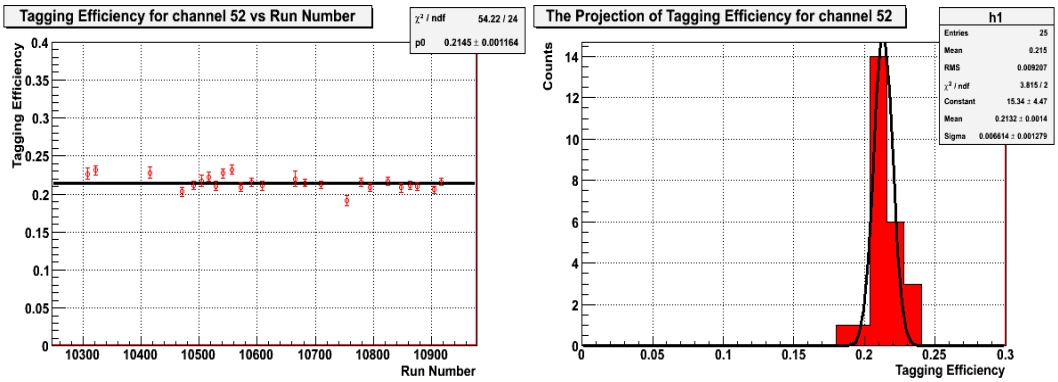

Figure 101: Tagging efficiency plots for FP channel 52.

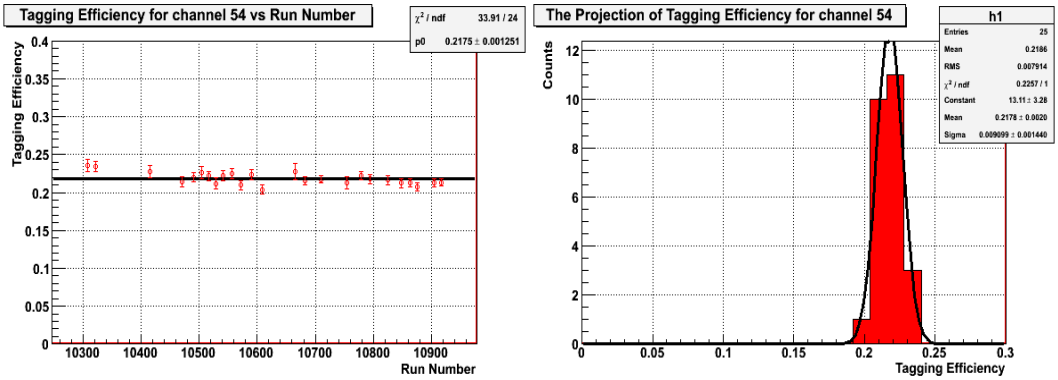

Figure 102: Tagging efficiency plots for FP channel 54.

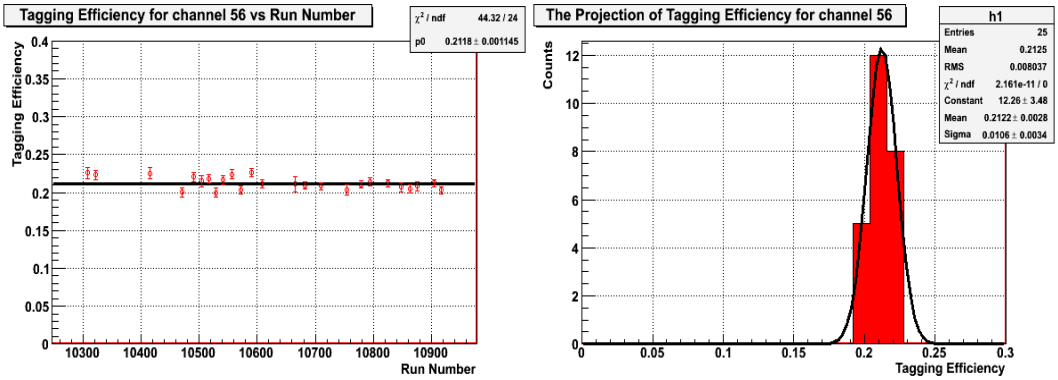

Figure 103: Tagging efficiency plots for FP channel 56.

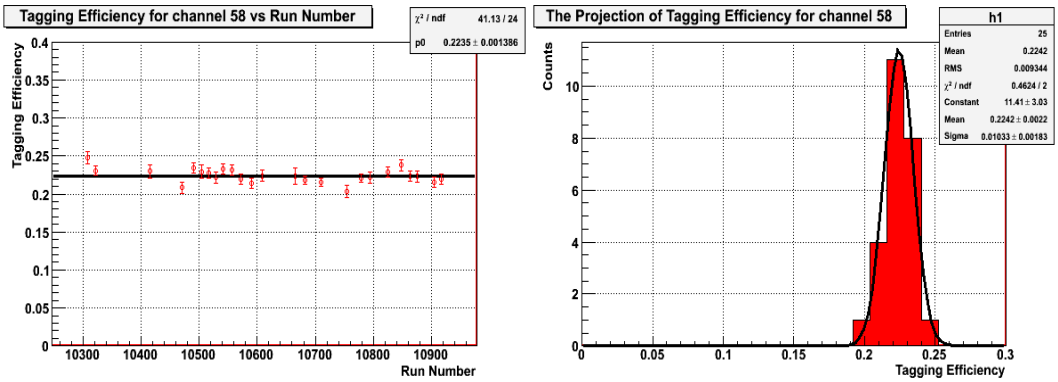

Figure 104: Tagging efficiency plots for FP channel 58.

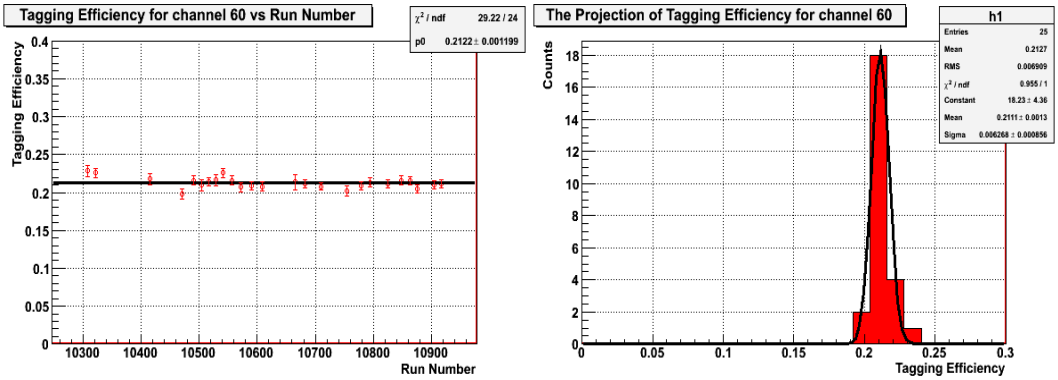

Figure 105: Tagging efficiency plots for FP channel 60.

D Tagging Efficiency from TiP

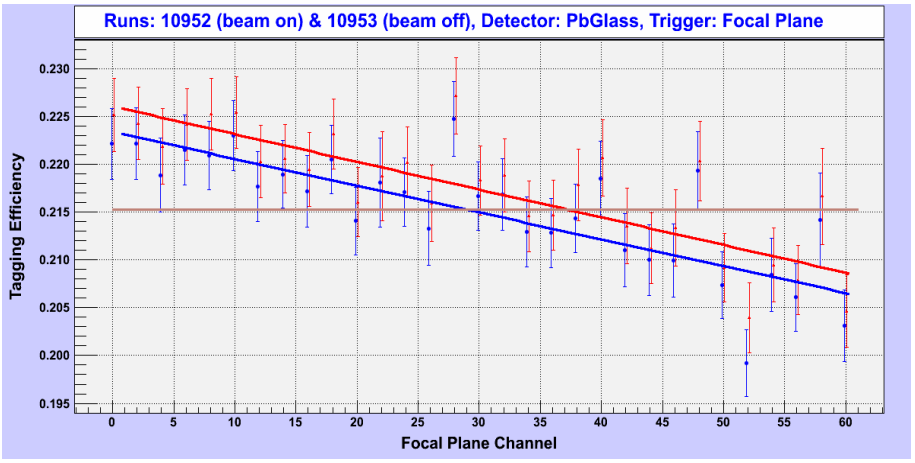

Figure 106: ϵ_{tagg} between 0 ms and 20 ms for the FP OR trigger.

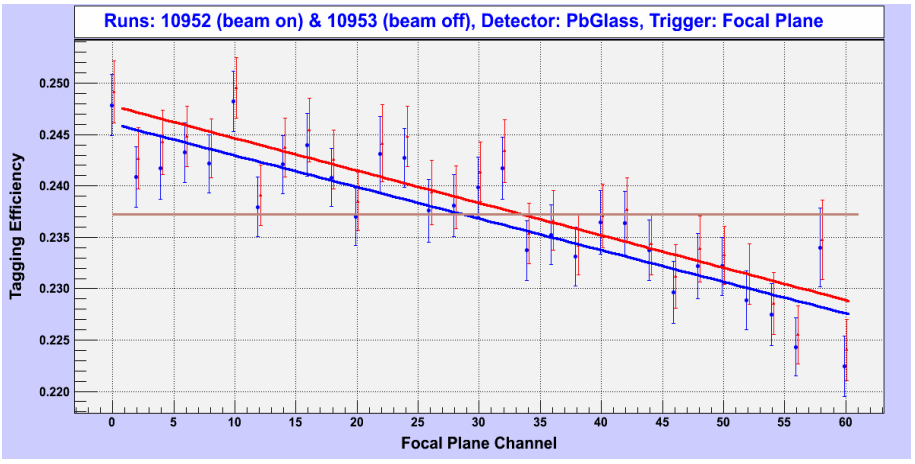

Figure 107: ϵ_{tagg} between 40 ms and 60 ms for the FP OR trigger.

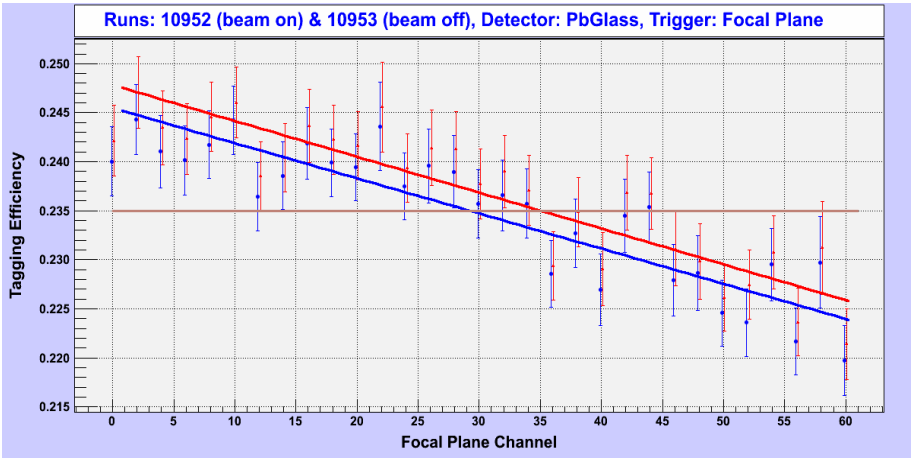

Figure 108: ϵ_{tagg} between 60 ms and 80 ms for the FP OR trigger.

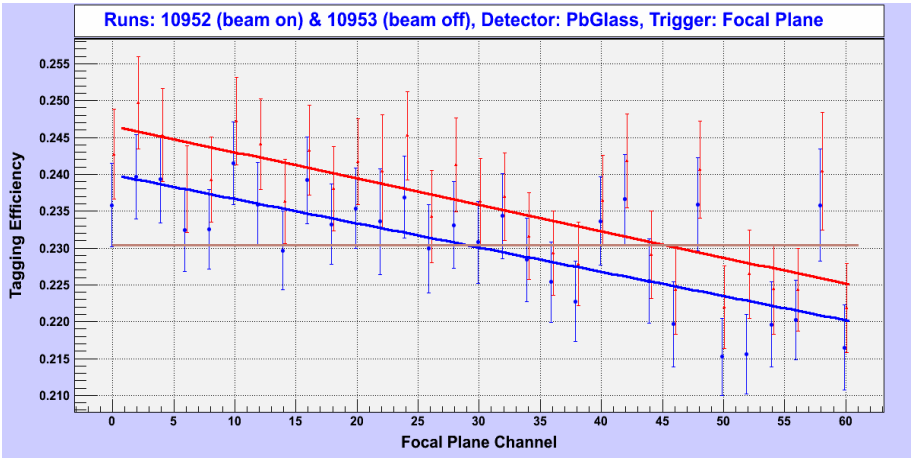

Figure 109: ϵ_{tagg} between 80 ms and 100 ms for the FP OR trigger.

Lund University, MAX-lab
Box 118, S-221 00 Lund
Visiting address: Ole Römers väg 1, Lund
Phone: +46 (0) 46 222 98 72, Fax: +46 (0) 46 222 47 10
E-mail: maxlab@maxlab.lu.se or
Firstname.Lastname@maxlab.lu.se
www.maxlab.lu.se